10-2023

Targeting SARS-CoV-2 main protease (Mpro) and human ACE-2: A virtual screening of carotenoids and polyphenols from tomato (Solanum lycopersicum L.) to combat Covid-19

Parvej Ahmad

Sahir Sultan Alvi
The University of Texas Rio Grande Valley, sahir.alvi@utrgv.edu

Inamul Hasan

M. Salman Khan

Recommended Citation

Ahmad, P., Alvi, S. S., Hasan, I., & Khan, M. S. (2023). Targeting SARS-CoV-2 main protease (Mpro) and human ACE-2: A virtual screening of carotenoids and polyphenols from tomato (Solanum lycopersicum L.) to combat Covid-19. Intelligent Pharmacy.

Intelligent Pharmacy xxx (xxxx) xxx

Contents lists available at ScienceDirect

Intelligent Pharmacy

journal homepage: www.keaipublishing.com/en/journals/intelligent-pharmacy

Targeting SARS-CoV-2 main protease (M^{pro}) and human ACE-2: A virtual screening of carotenoids and polyphenols from tomato (*Solanum lycopersicum* L.) to combat Covid-19

Parvej Ahmad [a,1], Sahir Sultan Alvi [a,b,1,*], Inamul Hasan [a], M. Salman Khan [a]

[a] *Integral Information & Research Center (IIRC-5), Clinical Biochemistry & Natural Product Research Lab, Department of Biosciences, Integral University, Lucknow, 226026, U.P., India*

[b] *Department of Immunology and Microbiology, South Texas Center of Excellence in Cancer Research, School of Medicine, University of Texas Rio Grande Valley, McAllen, 78504, Texas (TX), USA*

HIGHLIGHTS

- Human ACE-2 and SARS-CoV-2 M^{pro} facilitate viral invasion and replication.
- Antiviral efficacy of carotenoids and polyphenols from *S. lycopersicum* was studied.
- β-carotene and cyanidin are the best inhibitors of SARS-CoV-2 M^{pro} activity.
- α-carotene and cyanidin exhibited best ACE-2 inhibitory potential.
- RMSD, RMSF, SASA and Rg also validated the stable binding of ligand–target complex.

GRAPHICAL ABSTRACT

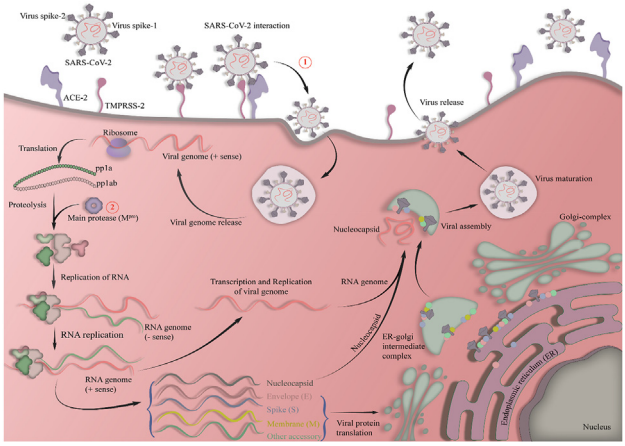

ARTICLE INFO

Keywords:
SARS-CoV-2
Main protease (M^{pro})
ACE-2

ABSTRACT

Background: Human angiotensin-converting enzyme-2 (ACE-2) and severe acute respiratory syndrome corona virus-2 (SARS-CoV-2) main protease (M^{pro}) have been established as the prime targets to restrict viral invasion and replication inside the host, respectively.

* Corresponding author. Department of Immunology and Microbiology, South Texas Center of Excellence in Cancer Research, School of Medicine, University of Texas Rio Grande Valley, McAllen, 78504, Texas (TX), USA.

E-mail addresses: contactpahmad@gmail.com (P. Ahmad), sahir.alvi@utrgv.edu (S.S. Alvi), yrinamul@gmail.com (I. Hasan), contactskhan@gmail.com (M.S. Khan).

Production and Hosting by Elsevier on behalf of KeAi

[1] These authors share equal authorship in this article.

https://doi.org/10.1016/j.ipha.2023.10.008
Received 3 September 2023; Received in revised form 23 October 2023; Accepted 23 October 2023
Available online xxxx

Please cite this article as: Ahmad P et al., Targeting SARS-CoV-2 main protease (M^{pro}) and human ACE-2: A virtual screening of carotenoids and polyphenols from tomato (*Solanum lycopersicum* L.) to combat Covid-19, Intelligent Pharmacy, https://doi.org/10.1016/j.ipha.2023.10.008

Carotenoids & polyphenols
Solanum lycopersicum L.
Covid-19
Hypertension

Methods: The current study delineated the SARS-CoV-2 M^{pro} as well as human ACE-2 inhibitory potential of carotenoids and polyphenols from tomato (*Solanum lycopersicum* L.) via *in-silico* interaction studies.
Results: Our drug-likeness studies showed that the selected carotenoids and polyphenols exhibited acceptable Lipinski's score and ADME determinants. Further, *in-silico* molecular modelling studies revealed that β-carotene, among other carotenoids, topped the binding score (ΔG: −6.75 kcal/mol; *Ki*: 11.32 μM) against SARS-CoV-2 M^{pro}, whereas, cyanidin was the best inhibitor of SARS-CoV-2 M^{pro} (−7.24 kcal/mol; *Ki*: 4.92 μM) amongst polyphenols. Similarly, α-carotene from carotenoids exhibited strongest human ACE-2 inhibitory activity (ΔG: −8.85 kcal/mol; *Ki*: 326.13 μM), whereas, cyanidin from polyphenols showed best binding affinity against human ACE-2 (ΔG: −7.24 kcal/mol; *Ki*: 4.89 μM). In contrast, 6-(ethylamino)-pyridine-3-carbonitrile, standard inhibitor of SARS-CoV-2 M^{pro}, exhibited comparatively weaker binding (ΔG: −4.78 kcal/mol; *Ki*: 267.49 μM), whereas, telmisartan (reference ACE-2 inhibitor) also exhibited lesser affinity (ΔG: −6.40 kcal/mol; *Ki*: 20.40 μM). Further exploration via MDS studies also validated the dynamic behavior and stability of protein-ligand complexes as evident by desirable RMSD, RMSF, Rg, and SASA.
Conclusion: The current study established carotenoids and polyphenols from *S. lycopersicum* L. as finer substitutes of reference standards against SARS-CoV-2 M^{pro} and human ACE-2 activity in combating SARS-CoV-2 infection.

1. Introduction

Over 4 years ago (in 2019), a novel coronavirus was recognized in China as a causative agent of unusual pneumonia with severe acute respiratory syndrome (SARS) and entitled novel SARS-CoV-2 while the respective disease was termed COVID-19. This newly emerged disease was later declared as serious global pandemic.[1,2] The RNA sequencing analysis of virus isolates from patients with unknown etiology depicted that the newly identified β-coronavirus had never been encountered before.[1] The novel SARS-CoV-2 constitutes ~80 % conserved genome with SARS-CoV, identified in 2002, and around 50 % with Middle East respiratory syndrome coronavirus (MERS-CoV) that was firstly identified in 2012.[3] Covid-19 has been regarded as the third internationally recognized pandemic of the twenty first century that is associated with coronaviruses in succession to SARS and MERS. The genomic organization of novel SARS-CoV-2 constitutes 14 open reading frames (ORFs) that can further be divided into two major classes *i.e.*, ORF1 (comprises of ORF1a and ORF1ab) and ORF2-14. The translation of ORF1a and ORF1ab produces polyproteins pp1a and pp1ab which are further processed by the viral proteases to give 16 non-structural proteins (NSP1-NSP16). On the other hand, ORF2-14 encode four structural proteins namely spike (S), envelope (E), membrane (M), and nucleocapsid (N). Moreover, 7 other ORFs related to accessory proteins were flanked by the above mentioned structural genes.[4] The majority of the proteins identified in SARS-CoV-2 share their structural features with the ones reported in the pathogenic SARS-CoV.[3]

Like other coronaviruses, the receptor binding domains (RBDs) of the spike glycoproteins (S) of SARS-CoV-2 are the key mediators which facilitate the angiotensin-converting enzyme-2 (ACE-2)-dependent invasion, the primary step of the infection process, and subsequent virulence of the viral particles into the host.[5,6] Therefore, the inhibition of the human ACE-2 has been established as the key strategies to combat the virulence of SARS-CoV-2.[7,8]

The most extensively exploited strategy to combat the virus replication is to consider essential proteins of the virus as potential inhibitory targets. The life cycle and virulence of the SARS-CoV-2 is attributed to the viral main protease (M^{pro}); the protein responsible for expression of viral genome.[9] The M^{pro} is also reckoned as $3CL^{pro}$ and Nsp5. It leads to the cleavage of the viral polyproteins into smaller counterparts together with both N- and C-terminal auto-processing sites.[10,11] Therefore, therapeutic blockage of SARS-CoV-2 M^{pro} so far has been considered the major therapeutic mechanisms and implied by distinct researchers across the globe to combat Covid-19.[10,12,13]

The SARS-CoV-2-triggered virulence results in disintegration of lung epithelium and co-stimulation of inflammatory responses which ultimately leads to the recruitment of immunological modulators at the site of injury and an altered and excessive immunological response ends up in serious pathologies of the lungs.[14,15] The SARS-CoV-2-mediated inflammatory response up-regulates the expression of various cytokines particularly, interleukin (IL)-1, IL-6, monocyte chemotactic protein-1 (MCP-1), and interferon-γ (IFN-γ), and such cytokine storm facilitates the accumulation of lymphocytes into the airway epithelium.[14,16,17] Considering the role of inflammation in the severity of SARS-CoV-2 infection, it would be of great importance to infer anti-inflammatory agents to cope with this deadly infection.

Owing to the adverse effects associated with synthetic drugs, the lead therapeutic agents from natural sources have been extensively studied for the treatment of distinct pathophysiological conditions *i.e.*, cardiovascular complications, diabetes, cancer, aging/neurological disorders, and inflammatory problems.[18–26] Similarly, *Solanum lycopersicum* L., commonly known as tomato, is one of the dietary supplements that are most popular and extensively consumed in the world. Numerous pharmacological studies have established the beneficial effects of direct or indirect intake of tomatoes and tomato-based foodstuffs against a number of sicknesses.[27–29] Most importantly, the potent therapeutic effects of *S. lycopersicum* L. has been attributed to the presence of significant content of various carotenoids (*i.e.*, lycopene, α-carotene, carotene, lutein, and phytofluene etc.) and polyphenols (*i.e.*, cyanidin, myricetin, delphinidin, quercetin, and caffeic acid etc.).[30–32]

However, we could not find any report demonstrating the protective role of the carotenoids and polyphenols from *S. lycopersicum* L. in combating SARS-CoV-2 infection via targeting viral M^{pro} and host ACE-2 activity. Therefore, considering the daily dietary consumption of tomato and its products with high antioxidant and anti-inflammatory properties, the current study was premeditated to test that whether the carotenoids and polyphenols from *S. lycopersicum* L. could be beneficial against the

Table 1
List of selected twenty-seven secondary metabolites from *S. lycopersicum L.*

S.N.	Compound name	PubChem ID (CID)	S.N.	Compound name	PubChem ID (CID)
	Carotenoids			Polyphenols	
1.	Lycopene	446925	14.	Naringenin chalcone	5280960
2.	Phytoene	5280784	15.	Rutin	5280805
3.	Phytofluene	6436722	16.	Quercetin	5280343
4.	β-carotene	5280489	17.	Chlorogenic acid	1794427
5.	γ-carotene	5280791	18.	Caffeic acid	689043
6.	Delta-carotene	5281230	19.	Naringenin	932
7.	Lutein	5281243	20.	Keamferol-3-rutinoside	122173234
8.	Neurosporene	5280789	21.	p-coumaric acid	637542
9.	α-carotene	4369188	22.	Ferulic acid	445858
10.	Neoxanthin	5281247	23.	Kaempferol	5280863
11.	Violaxanthin	448438	24.	Myricetin	5281672
12.	Antheraxanthin	5281223	25.	Cyanidin	128861
13.	Zeaxanthin	5280899	26.	Pelargonidin	440832
			27.	Delphinidin	128853

Table 2
Chemical properties of selected natural carotenoids and polyphenols from *S. lycopersicum L.*

S.N.	Compound name	PubChem ID (CID)	Log P	TPSA (Å^2)	M. Wt.	HBA	HBD	LPV	RT
Carotenoids									
1.	Lycopene	446925	8.53	15.56	536.87	0	0	2	16
2.	Phytoene	5280784	8.81	15.34	544.94	0	0	2	20
3.	Phytofluene	6436722	8.82	15.4	542.92	0	0	2	19
4.	β-carotene	5280489	7.79	13.54	536.87	0	0	2	10
5.	γ-carotene	5280791	8.3	14.52	536.87	0	0	2	13
6.	Delta-carotene	5281230	8.24	14.63	536.87	0	0	2	13
7.	Lutein	5281243	7.15	11.01	568.87	2	2	2	10
8.	Neurosporene	5280789	8.69	15.5	538.89	0	0	2	17
9.	α-carotene	4369188	7.83	13.65	536.87	0	0	2	10
10.	Neoxanthin	5281247	6.62	8.74	600.87	4	3	2	9
11.	Violaxanthin	448438	7.22	9.76	600.87	4	2	2	10
12.	Antheraxanthin	5281223	7.10	52.99	584.87	3	2	2	10
13.	Zeaxanthin	5280899	7.26	10.91	568.87	2	2	2	10
Polyphenols									
14.	Naringenin chalcone	5280960	1.03	2.82	272.25	5	4	0	3
15.	Rutin	5280805	2.43	−0.33	610.52	16	10	3	6
16.	Quercetin	5280343	1.63	1.54	302.24	7	5	0	1
17.	Chlorogenic acid	1794427	0.96	−0.42	354.31	9	6	1	5
18.	Caffeic acid	689043	0.97	1.15	180.16	4	3	0	2
19.	Naringenin	932	1.75	2.52	272.25	5	3	0	1
20.	Keamferol-3-rutinoside	122173234	2.79	0.02	594.52	15	9	3	6
21.	p-coumaric acid	637542	0.95	1.46	164.16	3	2	0	2
22.	Ferulic acid	445858	1.62	1.51	194.18	4	2	0	3
23.	Kaempferol	5280863	1.7	1.9	286.24	6	4	0	1
24.	Myricetin	5281672	1.08	1.18	318.24	8	6	1	1
25.	Cyanidin	128861	−2.59	1.94	287.24	6	5	0	1
26.	Pelargonidin	440832	−2.29	1.13	271.24	5	4	0	1
27.	Delphinidin	128853	−3.1	1.58	303.24	7	6	1	1
28.	[a]EPC	24701445	1.61	48.71	147.18	2	1	0	2
29.	[b] Telmisartan	56999	3.88	72.94	514.62	4	1	2	7

[a] Represents the reference standard antagonist of SARS-CoV-2 M^{pro} activity.
[b] Represents the reference standard antagonist of human ACE-2 activity. HBD: Hydrogen bond doner; HBA: Hydrogen bond acceptors; RT: Rotatable bonds; LPV: Lipinski Violation; EPC: 6-(ethylamino)pyridine-3-carbonitrile.

infection and virulence of SARS-CoV-2 via targeting human ACE-2-mediated invasion of viral particles and viral M^{pro} activities.

2. Methodology

2.1. Selection of carotenoids and polyphenols from Solanum lycopersicum L. as ligands

A set of twenty seven secondary metabolites (carotenoids & polyphenols) with antiviral potential from *Solanum lycopersicum* L. were selected through literature search[30] and summarized in Table 1.

2.2. Retrieval and processing of ligands 3D structures

The carotenoids & polyphenols were retrieved in.sdf files from PubChem database (https://pubchem.ncbi.nlm.nih.gov/). 6-(ethylamino) pyridine-3-carbonitrile (EPC) and telmisartan were used as reference standards against SARS-CoV-2 M^{pro} and human ACE-2 crystal structures, respectively. Interested ligands (3D-SDF files) were converted into PDB format before subjecting them to AutoDock 4.0. Further processing i.e., application of Char MM force field and energy minimization was done according to the standard procedures in Discovery studio.[33]

2.3. ADME and drug likeness studies of selected ligands

The selected carotenoids and polyphenols were screened for detailed analysis of physicochemical descriptors, drug likeness, and pharmacokinetics-associated variable *i.e.*, absorption, distribution, metabolism, and excretion (ADME) by using web-based tool as described previously[34] (http://www.swissadme.ch).

2.4. Analysis of toxicity of carotenoids and polyphenols from S. lycopersicum L

Following the ADME studies, the selected carotenoids and polyphenols were analyzed for the toxicity indices using ProTox-II.[34]

2.5. Retrieval and preparation of the SARS-CoV-2 M^{pro} and human ACE-2

The SARS-CoV-2 M^{pro} and human ACE-2 were retrieved from PDB using PDB IDs: 6Y84 and 1R42, respectively. The resolutions of these retrieved crystal structures were 1.39 Å and 2.20 Å, respectively, whereas, these structures were processed according to the standard protocol along with the prediction of active sites of both target proteins using DEEPSITE (https://www.playmolecule.com/).[31,35]

2.6. Molecular docking of carotenoids and polyphenols against SARS-CoV-2 M^{pro} and ACE-2

The grid dimensions for SARS-CoV-2 M^{pro} were 60 x 60 x 60 points with a grid spacing of 0.536 Å and grid center dimensions of 13.405, −1.7, and −2.1, respectively. Further, grid magnitudes of ACE-2 were 60 x 60 x 60 points having a grid spacing of 0.664 Å and grid center of 71.127, 68.18, and 31.8, respectively. The docking was done using Autodock 4.2 and the findings were obtained using Discovery Studio visualizer version 2020.[36,37]

2.7. Molecular dynamics simulation

To further explore the dynamic behavior of ligand–protein complexes, the best predicted hits (cyanidin, α-carotene, and telmisartan as a

Table 3
Interacting pattern of various carotenoids and polyphenols from *S. lycopersicum* L. against the crystal structure of SARS-CoV-2 M^{pro} (PDB ID: 6Y84).

S. No.	Compounds	Binding energy (ΔG: kcal/mol)	Inhibition Constant (Ki)	Interacting residues of SARS-CoV-2 M^{pro}
Carotenoids				
1.	β-carotene	−6.75	11.32 μM	Phe103, Val104, Arg105, Ile106, Gln110, Asn151, Ile152, Asp153, Ile249, Phe294
2.	α-carotene	−6.45	18.65 μM	Gln107, Pro108, Gln110, Asn151, Ile152, Asp153, Tyr154, Glu240, His246, Phe294, Arg298, Val303, Thr304
3.	Lutein	−6.14	31.76 μM	Pro009, Phe008, Arg105, Gln107, Gln110, Asn151, Ile152, Asp153, Tyr154, Arg298, Val303, Thr304
4.	Delta-carotene	−6.01	39.49 μM	Pro108, Lys109, Gln110, Ile200, Val202, Asn203, Glu240, Pro241, Asp245, His246, Asp248, Ile249, Pro293, Phe294
5.	Violaxanthin	−5.54	87.29 μM	Lys102, Val104, Ile106, Gln107, Gln 110, Asn151, Asp153, Asp155, Cys156, Ser158, Ile249, Phe294
6.	Neoxanthin	−5.50	93.58 μM	Lys102, Val104, Ile106, Gln110, Thr111, Asn151, Ile152, Asp153, Pro252, Phe294, Val297, Arg298
7.	γ-carotene	−5.30	129.31 μM	Lys100, Lys102, Val104, Ile106, Gln107, Pro108, Gly109, Gln110, Pro132, Asp153, Tyr154, Asp155, Cys156, Ile200, Thr201, Val202, Glu240, His246
8.	Zeaxanthin	−4.76	322.48 μM	Lys102, Val104, Ile106, Gln110, Thr111, Asn151, Asp153, Phe294, Val297, Arg298
9.	Phytofluene	−4.29	718.37 μM	Lys102, Phe103, Val104, Arg105, Ile106, Gln107, Gln110, Asn151, Ser158, Phe294, Val297, Arg298
10.	Antheraxanthin	−4.29	711.98 μM	Val104, Arg105, Ile106, Gln107, Gln110, Ile152, Asp153, Ser158, Phe294, Arg298,
11.	Neurosporene	−3.66	2.06 mM	Pro108, Gln110, Val202, Thr204, Glu240, Pro241, His246 Ile249, Phe294, Val297, Arg298
12.	Lycopene	−3.56	2.46 mM	Val104, Arg105, Ile106, Gln107, Gln110, Asn151, Ile152, Asp153, Asp248, Ile249, Phe294, Arg298
13.	Phytoene	−3.31	3.77 mM	

Table 3 (*continued*)

S. No.	Compounds	Binding energy (ΔG: kcal/mol)	Inhibition Constant (Ki)	Interacting residues of SARS-CoV-2 M^{pro}
				Val104, Ile106, Asn151, Ile152, Asp153, Ser158, Ile249, Phe294
Polyphenols				
14.	Cyanidin	−7.24	4.92 μM	Met006, Ala007, Phe008, Pro009, Gln127, Asp295, Arg298, Gln299, Val301, Gly302, Thr304
15.	Myricetin	−7.06	6.73 μM	Met006, Ala007, Phe008, Pro009, Gln127, Asp295, Gln299, Arg298, Gly302, Val303, Thr304,
16.	Delphinidin	−6.97	7.82 μM	Met006, Ala007, Pro009, Gln127, Asp295, Val296, Arg298, Gln299, Gly302, Val303, Thr304
17.	Pelargonidin	−6.96	7.86 μM	Met006, Phe008, Pro009, Gln127, Asp295, Gln299, Arg298, Gly302, Val303, Thr304
18.	Quercetin	−6.95	8.05 μM	Met006, Ala007, Phe008, Pro009, Gln127, Asp295, Arg298, Gln299, Gly302, Val303, Thr304,
19.	Kaempferol	−6.86	9.29 μM	Met006, Ala007, Phe008, Pro009, Gln127, Ile152, Tyr154, Asp295, Arg298, Gln299, Val303, Thr304,
20.	Rutin	−6.65	13.35 μM	Phe008, Lys102, Val104, Arg105, Ile106, Gln107, Gln110, Asn151, Ile152, Asp153, Ser158, Arg298,
21.	Naringenin	−6.60	14.55 μM	Met006, Ala007, Phe008, Pro009, Ile152, Tyr154, Phe291, Asp295, Gln299 Arg298, Val303, Thr304
22.	Chlorogenic acid	−6.22	27.78 μM	Lys102, Asn151, Ile152 Asp153, Ser158, Phe294, Val297, Arg298, Val303
23.	Keamferol-3-rutinoside	−5.95	43.29 μM	Phe008, Lys102, Asn151, Ile152, Asp153, Cys156, Ser158, Phe294, Arg298
24.	Naringenin chalcone	−5.27	137.07 μM	Met006, Phe008, Pro009, Gln127, Glu290, Phe291, Asp295, Arg298, Gln299, Gly302, Val303, Thr304,
25.	Caffeic acid	−4.38	619.50 μM	Arg105, Gln107, Ile106, Gln110, Thr111, Asn151, Thr292, Asp295, Arg298
26.	Ferulic acid	−4.23	787.54 μM	

(*continued on next page*)

Table 3 (*continued*)

S. No.	Compounds	Binding energy (ΔG: kcal/mol)	Inhibition Constant (Ki)	Interacting residues of SARS-CoV-2 M^{pro}
				Met006, Phe008, Pro009, Ile152, Asp153, Tyr154, Arg298, Val303, Thr304
27.	p-coumaric acid	−4.04	1.09 mM	Phe008, Pro009, Ile152, Asp153, Tyr154, Arg298, Val303, Thr304
28.	[a]EPC	−4.78	267.49 μM	Lys005, Met006, Phe008, Gln127, Glu290, Phe291, Asp295, Arg298, Gln299, Val303

[a] Represents the reference standard antagonist of SARS-CoV-2 M^{pro} activity; EPC: 6-(ethylamino)pyridine-3-carbonitrile.

positive control) with respect to 1R42 and (cyanidin, β-carotene and EPC) in respect to 6Y84 were selected to perform 50,000 ps all-atoms molecular dynamics simulation using GROningen MAchine for Chemical Simulations (GROMACS) package version 5.1.4.[37,38] To generate the molecular topology files for protein complex, we used CHARMM36 force field parameters, whereas, to create the topology of ligands, the CHARMM General Force Field (CGenFF) program server was used. The simulation system consists of TIP3P solvent model, dodecahedron box with the minimal distance of 1 nm between protein surface and edge of the box neutralized with the inclusion of Na + counter ions. For the energy minimization, the steepest descent algorithm was used for 50,000 steps with a cut-off value of 1000 kJ mol^{-1}. Bond lengths (all covalent bonds including Hydrogen atoms) were constrained using the Linear Constraint Solver (LINCS) algorithm. Equilibration phases were carried out for 100 ps NVT (constant number of particles, volume, and temperature) followed by 100 ps NPT (constant number of particles, pressure, and temperature) run. Temperature coupling was performed using a V-rescale thermostat, (a modified Berendsen-thermostat), for immersion at 300 K with a time constant of 0.1 ps, and pressure coupling was completed with a Parrinello-Rahman using a time constant of 2.0 ps.

The Verlet cut-off scheme was used for the non-bonded interactions (Lennard-Jones and Coulomb potentials) with a cut-off of 10 Å (1 nm). Particle-Mesh-Ewald (PME) algorithm was used for long-range electrostatic interactions with fourth-order cubic interpolation and 1.6 Å grid spacing. Production MD simulation was carried out for 10 ns.[37] The trajectory files for root-mean-square deviation (RMSD), root mean square fluctuation (RMSF), the radius of gyration (Rg), and solvent accessible surface area (SASA) were obtained using GROMACS with build-in trajectory tools (GROMACS files) and to quantify the strength of the molecular interaction between ligand-protein, non-bonded interaction energy was computed through Leonard–Jones and Columbic Interaction calculation in GROMACS. QtGrace program was used to plot data and analyze the simulation data.[38]

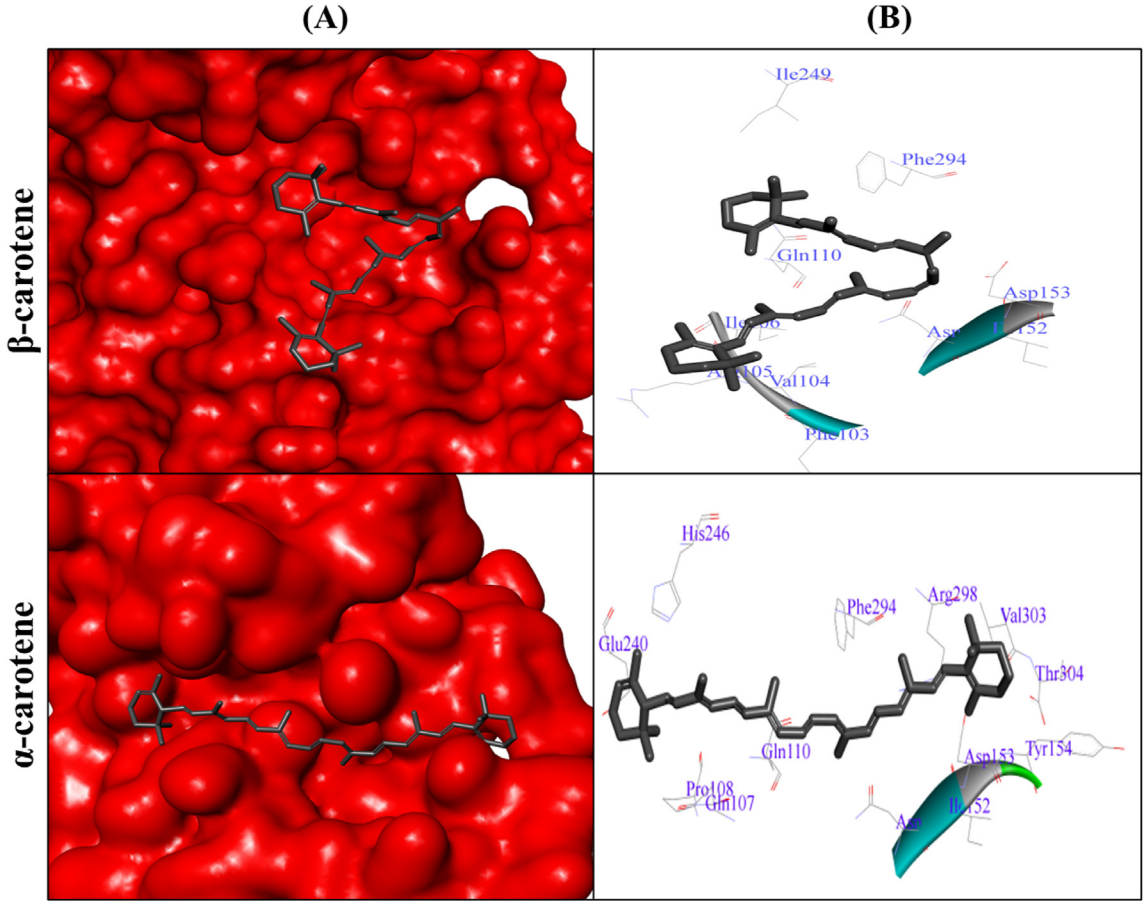

Fig. 1. *In-silico* binding patterns of carotenoids against SARS-CoV-2 M^{pro} (PDB ID: 6Y84) **(A)** Interactions of β-carotene and α-carotene are represented within the active pocket of SARS-CoV-2 M^{pro} (represented as surface structure) **(B)** 2D interactive poses (represented as ball and stick models) showing interaction with the amino acid residues of SARS-CoV-2 M^{pro}.

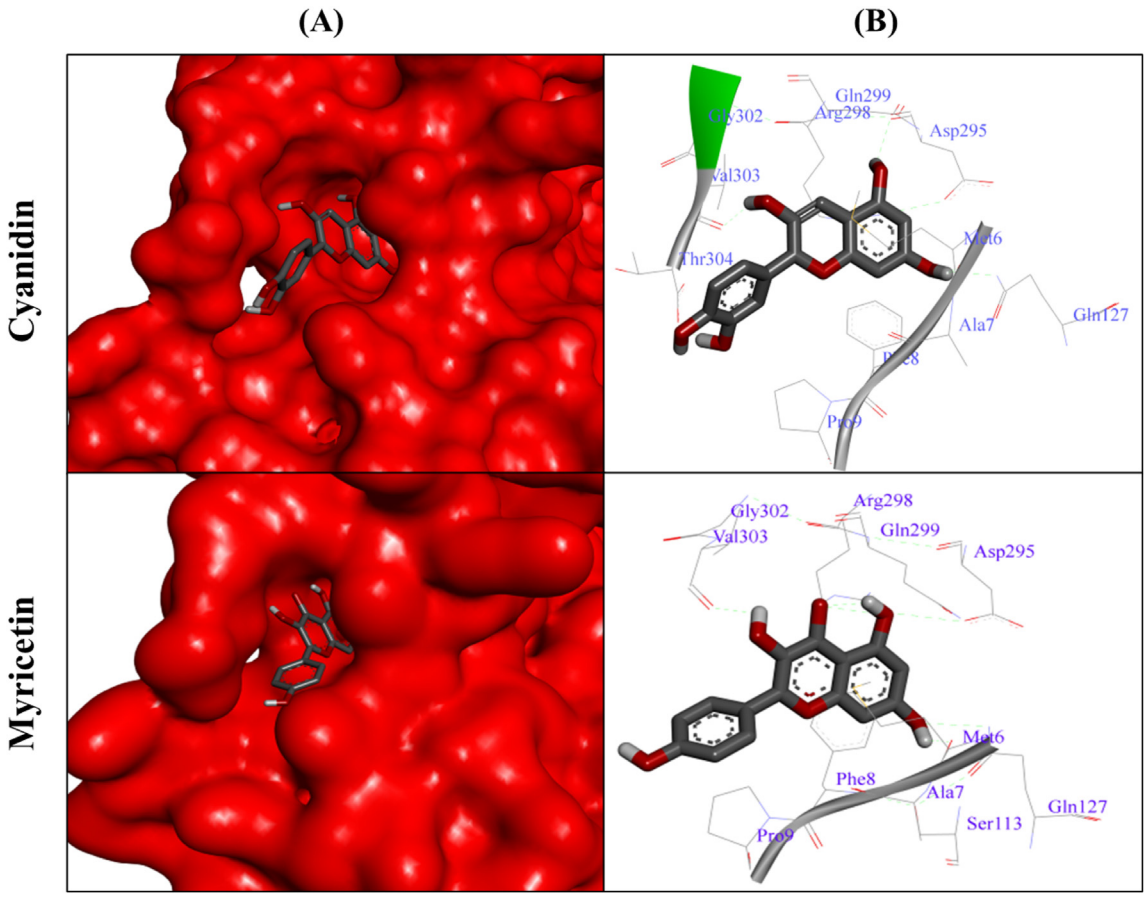

Fig. 2. *In-silico* binding patterns of polyphenols against SARS-CoV-2 M^{pro} **(A)** Interactions of cyanidin and myricetin are represented within the active pocket of SARS-CoV-2 M^{pro}. **(B)** 2D interactive poses showing their interaction with the amino acid residues of active pocket of SARS-CoV-2 M^{pro}.

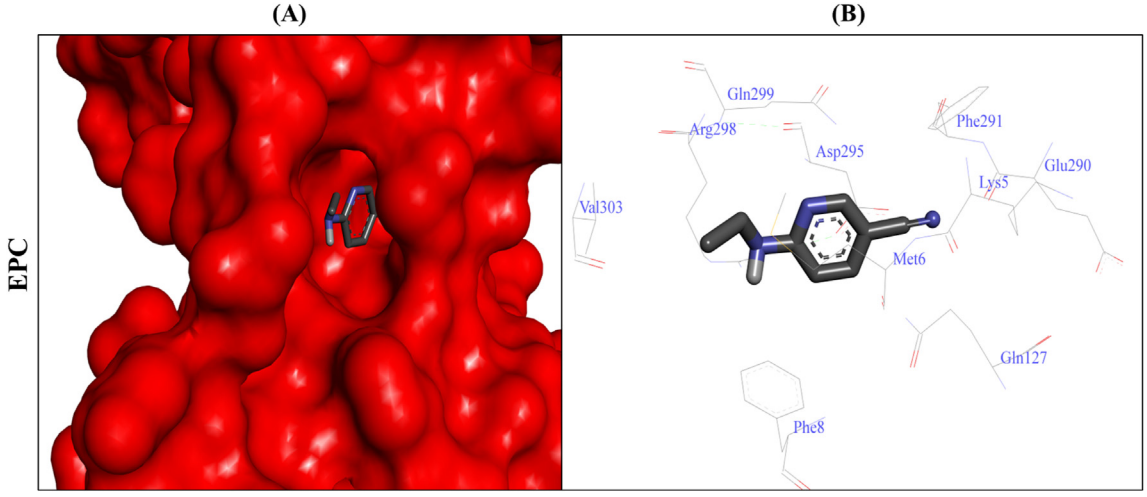

Fig. 3. *In-silico* binding patterns of EPC against the SARS-CoV-2 M^{pro} **(A)** Interaction of EPC is represented within the active pocket of SARS-CoV-2 M^{pro}. **(B)** 2D interactive pose of EPC showing its interaction with the amino acid residues of active pocket of SARS-CoV-2 M^{pro}.

3. Results and discussion

3.1. Drug-like properties of carotenoids and polyphenols from S. lycopersicum L

The drug-discovery program constitutes the evaluation of a series of factors to identify the drug-likeness of chemical libraries. In this regard, distinct computer-aided strategies *i.e.*, Lipinski's rule of five are being implied.[39,40] Similarly, in the current study, we opted AI-based strategies to predict the drug-likeness of selected carotenoids as well as polyphenols from *S. lycopersicum* L. The Lipinski's Rule of Five includes molecular weight (M.W.≤500 Da), H-bond donors (HBD≤5), H-bond acceptors (HBA≤10) and octanol–water partition coefficient (LogP≤5). Our drug-likeness analysis portrayed that selected carotenoids and polyphenols fall under the acceptable scores of Lipinski's rules of five with a few exceptions. Particularly, the chemical structure of rutin exhibited 16

Table 4
Interacting pattern of various carotenoids and polyphenols from *S. lycopersicum* L. against the crystal structure of human ACE-2 (PDB ID: 1R42).

S. No.	Compounds	Binding energy (ΔG: kcal/mol)	Inhibition Constant (*Ki*)	Interacting residues of human ACE-2
Carotenoids				
1.	α-carotene	−8.85	326.13 nM	Asp67, Ser70, Ala71, Leu73, Lys74, Leu95, Gln98, Ala99, Leu100, Gln102, Asp206, Leu391, Lys562
2.	γ-carotene	−8.61	490.01 nM	Leu95, Gln98, Gln102, Ser105, Asn117, Leu120, Asn121, Ser124, Lys187, Tyr196, Tyr202, Gly205, Asp206, Glu208, Val209, Ala396, Ser507, Asn508, Asp509, Lys562, Glu564, Pro565, Trp566,
3.	β-carotene	−7.79	1.95 μM	Phe32, Phe40, Ser43, Gly66, Trp69, Ser70, Leu73, Ala99, Trp349, Asp350, Phe390, Leu391, Arg393
4.	Lutein	−7.49	3.21 μM	Phe40, Leu85, Gln98, Ala99, Gln102, Asn194, His195, Tyr196, Asp350, Asp382, Tyr385, Phe390, Leu391, Arg393, Asn394,
5.	Violaxanthin	−7.48	3.48 μM	Ala99, Leu73, Leu95, Gln98, Leu100, Gly205, Asp206, Ala348, Trp349, Asp350, Asp382, Phe390, Leu391, Arg393, Asn394, His401, Lys562
6.	Neoxanthin	−6.47	19.63 μM	Phe40, Ser44, Ser47, Gly66, Trp69, Ser70, Ala348, Trp349, His378, Asp382, Leu391, Phe390, Arg393 Asn394, His401,
7.	Lycopene	−5.76	59.62 μM	Phe40, Ser44, Leu73, Lys74, Ala99, Leu100, Ala348, Trp349, Asp350, Asp382, Phe390, Leu391, Asn394,
8.	Phytoene	−5.43	104.43 μM	Phe40, Ala99, Gly205, Asp206, Glu208, Val209, Thr347, Ala348, Asp350, Glu375, His378, Asp382, Phe390, Leu391, Arg393, Asn394, Ala396, His401, Lys562, Pro565, Trp566,
9.	Neurosporene	−5.27	136.18 μM	Ser44, Ser70, Leu73, Lys74, Ser77, Ala99, Leu100, Glu110, Phe390, Leu391, Arg393, Asn394,
10.	Zeaxanthin	−4.99	219.60 μM	Trp69, Leu73, Ser77, Ala99, Leu100, Gln102, Asn103, Gly104, Ser105, Tyr202, Gly205, Phe390, Leu391, Lys562
11.	Delta-carotene	−4.70	357.08 μM	Phe40, Ser47, Asn51, Met62, Thr347, Ala348, Trp349, Asp350, Asp382, Phe390, Arg393,
12.	Antheraxanthin	−4.49	511.45 μM	Trp69, Asn117, Leu120, Asn121, Ser124, Tyr202, Phe390, Leu391, Arg393, Asn394, Asn508, Asp509
13.	Phytofluene	−3.51	2.66 mM	Trp69, Leu73, Ala99, Asp206, Glu375, His378, Phe390, Leu391, Asn394, Gly395, Asn397, Glu398, His401, Glu402, Arg514,
Polyphenols				
14.	Cyanidin	−7.24	4.89 μM	Leu91, Leu95, Asp206, Tyr207, Glu208, Val209, Asn210, Gly211, Val212, Ala395, Asn397, Lys562, Ser563, Glu564, Pro565, Trp566
15.	Kaempferol	−6.61	14.23 μM	Gln102, Tyr196, Tyr199, Tyr202, Trp203, Gly205, Asp206, Glu398, Asp509, Tyr510, Ser511, Arg514,
16.	Naringenin	−6.46	18.46 μM	Gln102, Tyr196, Tyr199, Tyr202, Trp203, Gly205, Asp206, Glu398, Asp509, Tyr510, Ser511, Arg514
17.	Chlorogenic acid	−6.44	19.23 μM	Phe40, Trp349, Asp350, Asp382, Tyr385, Phe390, Leu391, Arg393, Asn394, Lys562
18.	Rutin	−6.41	19.99 μM	Phe40, Trp69, Ala99, Gln102, Asp206, Phe390, Leu391, Leu392, Arg393, Lys562,
19.	Quercetin	−6.23	27.35 μM	Phe40, Trp69, Leu73, Asp350, Asp382, Tyr385, Phe390, Leu391, Leu392, Arg393, Asn394, His401
20.	Myricetin	−5.98	41.59 μM	Leu95, Gln98, Ala99, Gln102, Tyr196, Gly205, Asp206, Ala396, Asn397, Lys562, Glu564, Trp566,
21.	Delphinidin	−5.91	46.25 μM	Gln81, Gln98, Ala99, Gln101, Gln102, Asn103, Val107, Asn194, His195, Tyr196, Ala193,
22.	Keamferol-3-rutinoside	−5.88	49.10 μM	Asp30, Asn33, His34, Thr92, Val93, Gln96, Ala386, Gln388, Pro389, Arg393
23.	Pelargonidin	−5.18	158.27 μM	Lys26, Leu29, Asp30, Asn33, His34, Val93,

(*continued on next page*)

Table 4 (*continued*)

S. No.	Compounds	Binding energy (ΔG: kcal/mol)	Inhibition Constant (*Ki*)	Interacting residues of human ACE-2
				Gln96, Ala386, Ala387, Gln388, Pro389, Arg393
24.	Naringenin chalcone	−4.71	352.17 μM	Gln102, Tyr196, Tyr202, Trp203, Gly205 Asp206, Glu208, Val209, Ala396, Lys562, Pro565, Trp566
25.	p-coumaric acid	−4.69	366.57 μM	Lys94, Leu95, Gln98, Glu208, Val209, Asn210, Ala396, Lys562, Glu564, Pro565, Trp566
26.	Caffeic acid	−3.83	1.55 mM	Lys26, Leu29, Asp30, Asn33, Asn90, Gln96, Pro389
27.	Ferulic acid	−3.77	1.74 mM	Lys26, Leu29, Asp30, Asn33, Asn90, Gln96, Pro389
28.	[a]Telmisartan	−6.40	20.40 μM	Gln102, Tyr196, Trp203, Glu205, Asn394, Gly395, Ala396, Asn397, Glu398, Tyr510, Ser511, Arg514, Lys562

[a] Represents reference standard antagonist of human ACE-2.

HBA as well as 10 HBD, whereas, keamferol-3-rutinoside also violated Lipinski's rules with 15 HBA and 9 HBD (Table 2). The reference standard EPC exhibited 2 HBA and 1 HBD, while telmisartan possessed 4 HBA and 1 HBD. In contrast, it is well reckoned that carotenoids are long chain hydrocarbons (no. of carbons >40) with or without unsaturated bonds and exhibit very high molecular weight (M.W. > 500 Da).[31,32] An ample of studies have investigated the cytotoxicity and toxicity of naturally occurring carotenoids (with high M.W.) and concluded that even very high doses of carotenoids did not produce any toxic effect on the cells, animal models as well as humans.[28,41] Hence, based on these remarks, we ruled out the M.W. criteria for the assessment of the drug-likeness of the selected carotenoids. On the other hand, amongst 14 of the selected polyphenolic compounds from the *S. lycopersicum* L., only 2 exhibited the M.W. greater than 500 Da (rutin: 610.52 and keamferol-3-rutinoside: 594.52 Da). In contrast, the M.W. of the reference standard drugs EPC and telmisartan was found to be 147.18 and 514.62 Da, respectively. Here, the higher M.W. of telmisartan (>500 Da) further explains the fact that a chemical entity violating the M.W. criterion may also become a standard therapeutic drug candidate.

In addition, considering the influence of hydrophobic interactions in drug–target interaction, the topological polar surface area (TPSA) is used as the measure of the polarity and permeability of compounds across the membrane.[42,43] The results of our LogP analysis showed that all the carotenoids have LogP values greater than 5, whereas, the desirable threshold for LogP is ≤ 5). In contrast, all the polyphenols showed LogP values less than 5 (ranging from −3.1 to 2.79) (Table 2). The increased LogP values for all the carotenoids (maximum LogP: 8.82 for phytofluene) could be explained by the fact that carotenoids are highly hydrophobic or lipophilic in nature and have high possibility of membrane fusion and transport, as high Log *P* values are associated with increased lipophilicity.[44] Their hydrophobicity results in increased persistence and bioavailability due to decreased excretion through urination and hence, enhanced bioavailability as well as high pharmacological efficiency.[27] On the other hand, the LogP values for the reference standards EPC and telmisartan were found to be 1.61 and 3.88, respectively.

Unlike LogP values, all the selected carotenoids (8.74–52.99) as well as polyphenols (−0.42 to 2.82) exhibited desired TPSA thresholds (TPSA <100 Å^2) as established by previous studies.[45] More interestingly, values of TPSA less than 60–70 Å^2 are considered ideal for the drugs used to treat central nervous system disorders.[45] The observations from the current study are signifying the potential of selected carotenoids as well as polyphenols for the treatment of CNS disorders. These findings are clearly advocating that carotenoids and polyphenols qualify drug-likeness barrier and can be investigated for further pharmacological effects. Most importantly, the TPSA of selected carotenoids and polyphenols was far better than that of the reference standards EPC and telmisartan which exhibited the TPSA of 48.71 and 72.94 Å^2, respectively.

3.2. Carotenoids and polyphenols have acceptable ADME variables

The ADME analysis depicted that the selected carotenoids exhibit very low Aq. Solubility (ranging from 0.00 to 8.57 mg/L for zeaxanthin and phytoene, respectively), however, polyphenols showed very high Aq. Solubility from 10.17 mg/L for keamferol-3-rutinoside to 817291 mg/L for chlorogenic acid. The poor Aq. Solubility of the carotenoids has been attributed to the hydrophobic nature of long hydrocarbon chains.[27,32] In contrast, the very high solubility of polyphenols selected in this study could be explained by the higher number of HBs formed by the polyphenols in Aq. Solutions (Table 2 and Supplementary Table S1). The Aq. solubility of the reference standard EPC was 448.37 mg/L whereas telmisartan showed very poor Aq. solubility 0.49 mg/L. On the other hand, blood brain barrier (BBB) penetration score for all carotenoids ranged from 9.01 for neoxanthin to 27.75 C. Brain/C. Blood for phytoene, which was greater than the threshold of 2. These findings further signified the implications of these carotenoids for the management of CNS-related pathologies as drug candidates having BBB score >2.0, between 2.0–0.1 and < 0.1 reflect high, moderate and low absorption across BBB, respectively.[46,47] Conversely, the BBB score for selected polyphenols ranged from 0.0285 to 0.76 (C. Brain/C. Blood) which reflects their either low or moderate absorption across BBB. Among all polyphenols, rutin and ferulic acid showed lowest and highest absorption across BBB, respectively (Supplementary Table S1). The BBB score for EPC and telmisartan was 0.5935 and 1.283, respectively, which signifies their moderate absorption across BBB.

Similarly, the determination of Caco-2 and MDCK cells permeability in drug discovery is thought to be a critical step.[47–49] The PreADME investigation showed that carotenoids have Caco-2 permeability range of 23.225 (for β-carotene) to 54.921 nm/Sec (for lutein), whereas, the Caco-2 permeability for polyphenols was found to be 0.375 nm/Sec (for delphinidin) to 21.11 nm/Sec (for p-coumaric acid) (Supplementary Table S1). Similarly, the MDCK cell permeability for carotenoids ranged between 0.055 nm/Sec for violaxanthin to 67.975 nm/Sec for phytofluene, whereas, polyphenols showed higher MDCK cell permeability than that of carotenoids (0.251–228.56 nm/Sec). These findings are advocating the protective nature of these polyphenols due to their high permeability across Caco2 and MDCK cells for the treatment and management of epithelial injury, particularly in case of SARS-CoV-2 infection which primarily targets the lung epithelium. The Caco2 cell permeability of reference standard EPC and telmisartan was found to be 0.29 and 34.55 nm/Sec, respectively, whereas the MDCK cell permeability of EPC and telmisartan was 72.92 and 0.46 nm/Sec, respectively. The permeability scores <4, 4<70, and >70 (nm/Sec) suggest low, middle, and high permeability, respectively.[50]

In addition, the importance of assessment of transdermal permeability of drug candidates in drug discovery cannot be denied.[51] In this order, all the carotenoids exhibited negative logKp values (−0.805 cm/h for violaxanthin to −0.607 cm/h for phytoene) which fall under the desirable range of logKp for drug candidates (Supplementary Table S1).[52] This efficient transdermal permeability of carotenoids could have been achieved via their high hydrophobicity and membrane-fusion ability.[32] Similarly, polyphenols also showed significant skin permeability scores (−4.667 for rutin to −1.71 cm/h for p-coumaric acid) (Supplementary Table S1). On the other hand, the logKp value for EPC and telmisartan

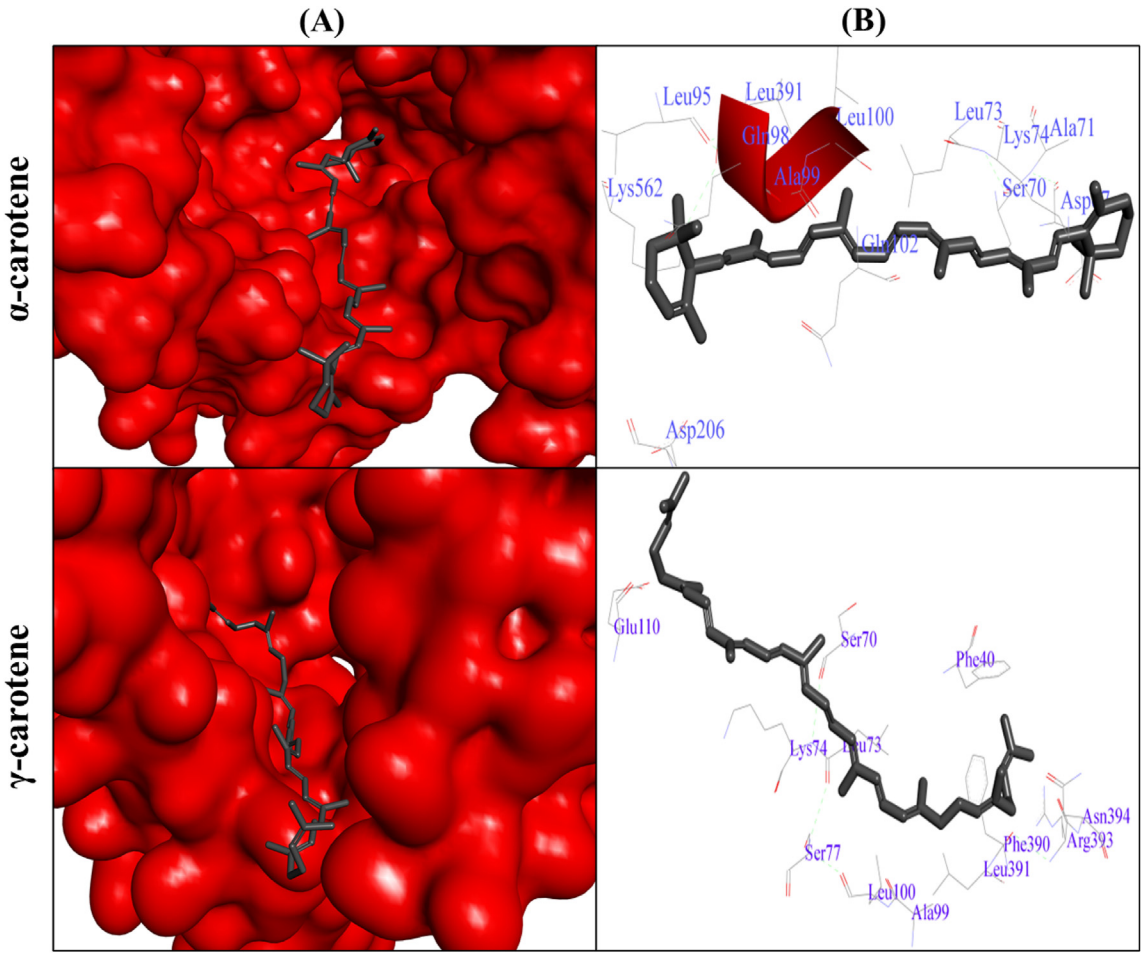

Fig. 4. *In-silico* binding patterns of carotenoids against human ACE-2 (PDB ID: 1R42) **(A)** Interaction of α-carotene and γ-carotene are represented within the active pocket of human ACE-2 (represented as surface structure) **(B)** 2D interactive poses (represented as ball and stick models) showing their interaction with the amino acid residues of active pocket of human ACE-2.

was recorded to be −2.042 and −2.017 cm/h, respectively. On the other hand, the plasma protein binding (PPB) plays a crucial role in the distribution of a drug from circulation to the target organs. Drugs with extensive PPB reflect a low volume of distribution (Vdss), long plasma half-lives ($T_{1/2}$), and may incur lower hepatic and renal clearance.[53,54] The PPB efficacy of carotenoids ranged from 91.27 % (for violaxanthin) to 100 % (for α, β, and γ carotenes), while the PPB of polyphenols ranged from 40.29 % to 100.00 %, suggestive of persistent pharmacological effects. The reference standard, EPC showed a poor PPB of 20.78 % only while telmisartan exhibited comparatively higher PPB ability (92.75 %).

Parallelly, the efficiency of drug relies on their human intestinal absorption (HIA) to the distribution to target organs where the HIA range between 0 and 29 %, 30–79 %, and 80–100 % are considered low, middle and high, respectively.[55] The predicted % HIA of all the carotenoids screened in this study ranged from 95.17 to 100.00 % (09 among 13 carotenoids exhibited 100 % HIA), whereas, HIA for polyphenols ranged from 2.86 to 92.09 % and most of them exhibited HIA more than 50 % (Supplementary Table S1). This high HIA signifies the enhanced bioavailability of these carotenoids as well as polyphenols, which might be attributed to potent pharmacological actions of these secondary metabolites. On the other hand, the HIA for reference M^{pro} inhibitor (EPC) and ACE-2 inhibitor (telmisartan), was 93.18 % and 98.08 %, respectively, which ultimately reflects the higher intestinal absorption of these standard inhibitors.

Interestingly, the cytochrome P450 2D6 or CYP2D6 mediates around 25 % of total metabolism and clearance of the drugs after administration.[56,57] The degree of CYP2D6-functionality diverges among individuals and hence categorized into either ultra- and poor-metabolizers. Where, the former once exert rapid drug metabolism and therapeutic effects, while the latter once exert persistent drug effectiveness as well as low clearance rates.[57,58] These observations established CYP2D6-mediated drug metabolism as a major factor in dose adjustment.[59] In this attempt, our results depicted that neither the carotenoids nor polyphenols exhibited CYP2D6 inhibitory activity. These findings suggested that the selected carotenoids and polyphenols exhibit instant metabolism and excretion which might be attributed to their substantial pharmacological effects as well as diminished toxicity. On the other hand, all the carotenoids were nonreactive against CYP2D6 and only three of the selected polyphenols namely, cyanidin, delphinidin, and pelargonidin acted as CYP2D6 substrate which further validate their speedy metabolism, instant therapeutic actions as well as clearance from the body. Similarly, EPC and telmisartan also did not inhibit the CYP2D6 activity however EPC may weakly act as a substrate for CYP2D6. These findings are well justified by recently published reports concerning the bioavailability and here-mentioned fate of administered drugs.[57,60]

3.3. Carotenoids and polyphenols are non-toxic

Distinct pharmacological entities are analyzed using AI-based approaches.[27,28] In the same vein, we implied ProTox-II, a web-based platform, to envisage various important determinants of drug toxicity and safety (Supplementary Table S2). Our results showed that most of the selected carotenoids exerted very high LD_{50} values (up to 5700 mg/kg) except a very few which showed lower LD_{50} values (10–55 mg/kg).

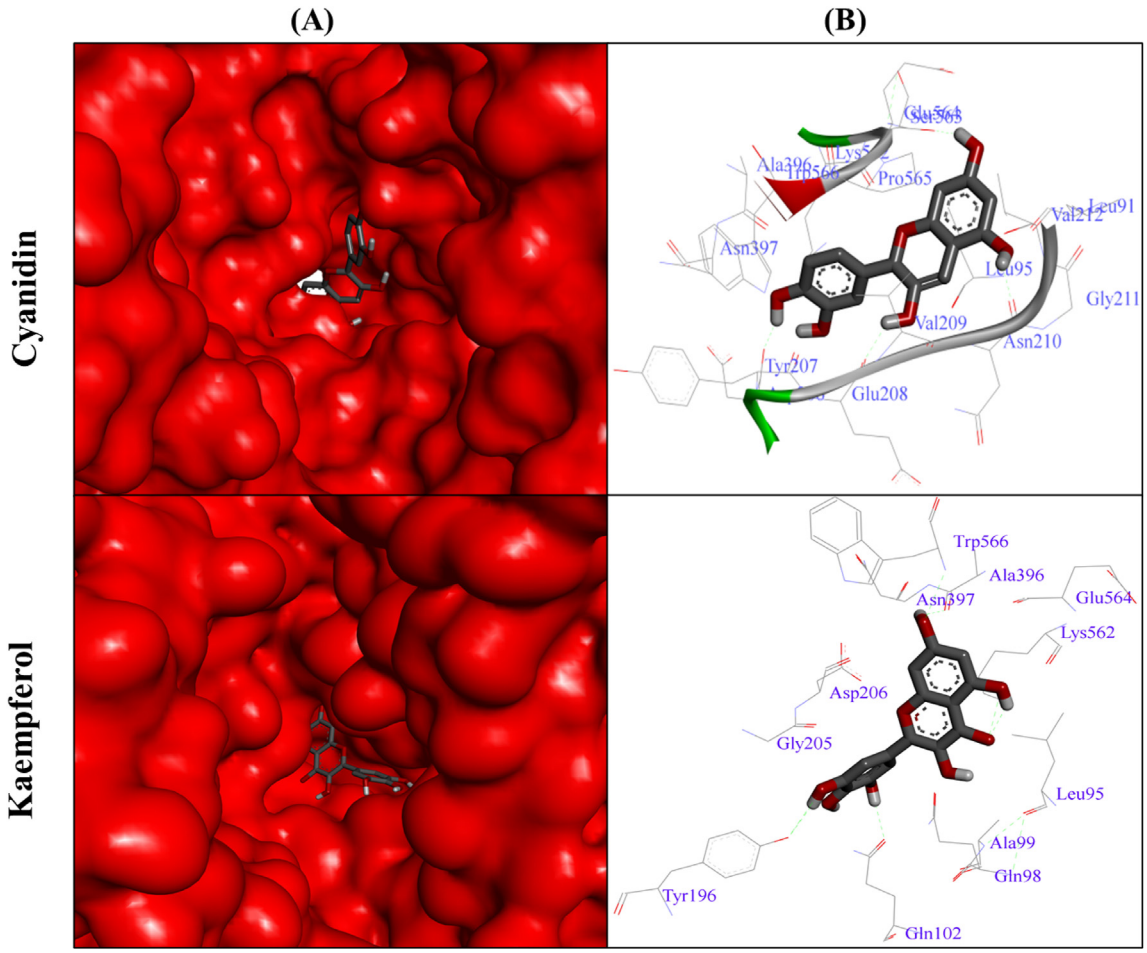

Fig. 5. *In-silico* binding patterns of polyphenols against human ACE-2 **(A)** Interactions of cyanidin and kaempferol are represented within the active pocket of human ACE-2. **(B)** 2D interactive poses showing their interaction with the amino acid residues of active pocket of human ACE-2.

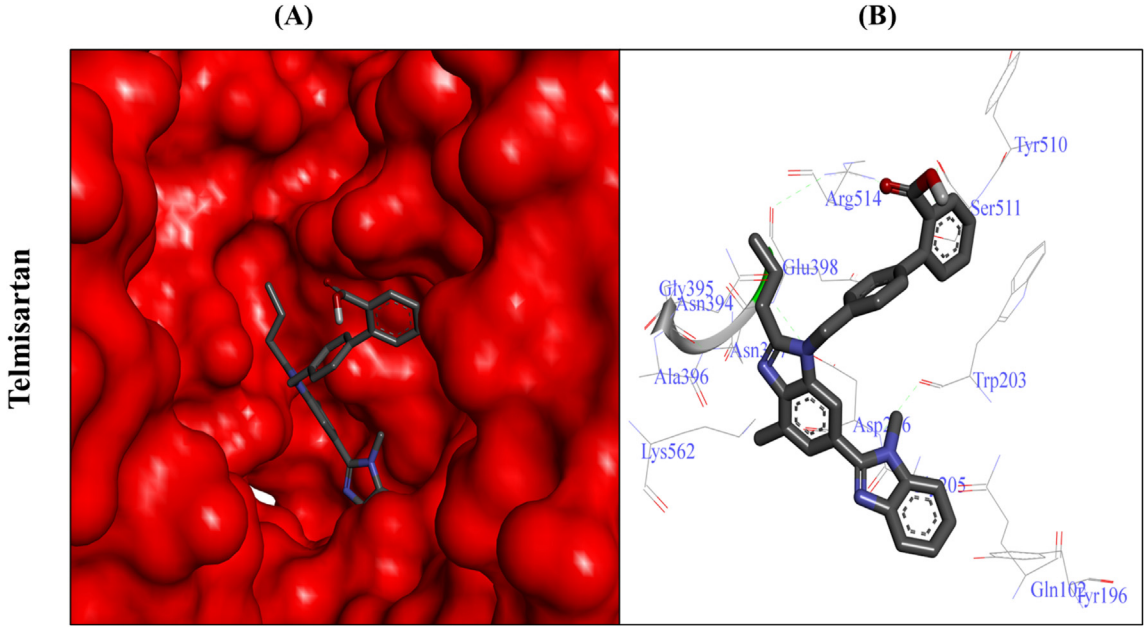

Fig. 6. *In-silico* binding patterns of telmisartan against human ACE-2 **(A)** Interaction of telmisartan is represented within the active pocket of human ACE-2. **(B)** 2D interactive pose of telmisartan showing its interaction with the amino acid residues of active pocket of human ACE-2.

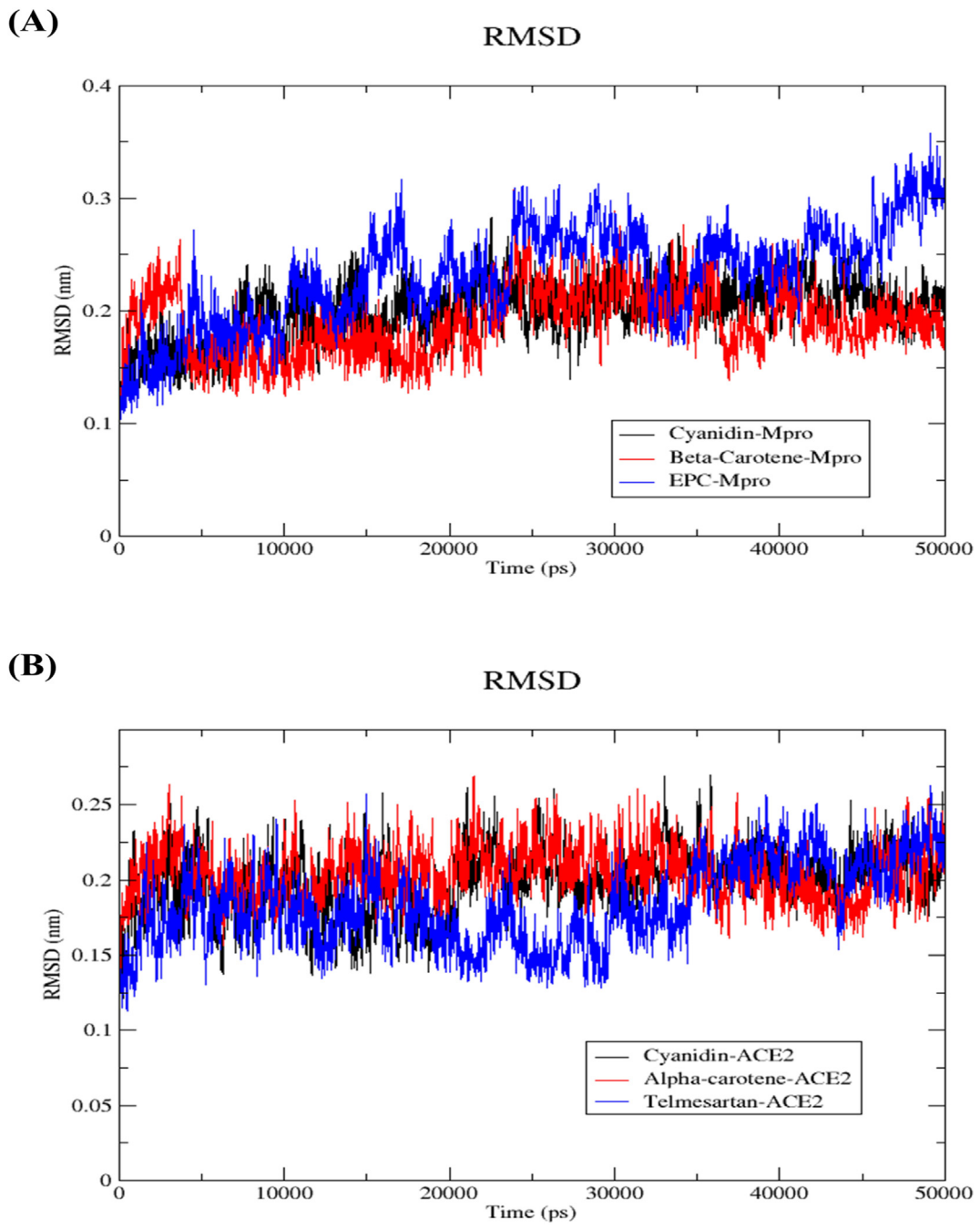

Fig. 7. **(A)** Plots of RMSD values for the backbone atoms of the Cyanidin-6Y84, Beta-carotene-6Y84 and EPC-6Y84 complexes from initial structures throughout the 50,000 ps simulation. **(B)** Plots of RMSD values for the backbone atoms of the cyanidin-1R42, alpha-carotene-1R42, and telmisartan-1R42 complexes from initial structures throughout the 50,000 ps simulation.

Polyphenols also showed very high LD_{50} values (1190–5000 mg/kg). However, reference SARS-CoV-2 M^{pro} inhibitor EPC showed a lower LD_{50} of 330 mg/kg (drug toxicity class: 3), whereas, the LD_{50} for reference ACE-2 inhibitor telmisartan was predicted to be 500 mg/kg (drug toxicity class: 4). On the other hand, the top scoring carotenoids fall under the drug toxicity class 6 ($LD_{50} > 5000$ mg/kg), 5 and 4 which are considered as non-toxic for animals as per the globally harmonized system (GHS) of classification of labelling of chemicals.[47] On the other hand, ten out of fourteen polyphenols fall under the drug toxicity class 5 (LD_{50} 2000–5000 mg/kg). These results clearly depict that selected carotenoids and polyphenols are non-toxic and safe for therapeutic drug development programs. The GHS approach has previously been implied to predict the safety of test compounds.[47]

3.4. SARS-CoV-2 M^{pro} active pocket is occupied by carotenoids and polyphenols from S. lycopersicum L

Owing to the determining role in the proteolysis of viral polyproteins, the M^{pro} of the SARS-CoV-2 has been established as the preferred target in combating its virulence.[61,62] Similarly, we also used SARS-CoV-2 M^{pro} as the major target via selected carotenoids as well as polyphenols for the management of this deadly outbreak. In this attempt, our molecular docking studies revealed a strong interaction of nearly all the selected carotenoids with binding affinities (ΔG) −6.75 to −3.31 kcal/mol against the active pocket of SARS-CoV-2 M^{pro} (Table 3). Among other carotenoids, β-carotene topped the binding score (ΔG: −6.75 kcal/mol) and interacted with Phe103, Val104, Arg105, Ile106, Gln110, Asn151,

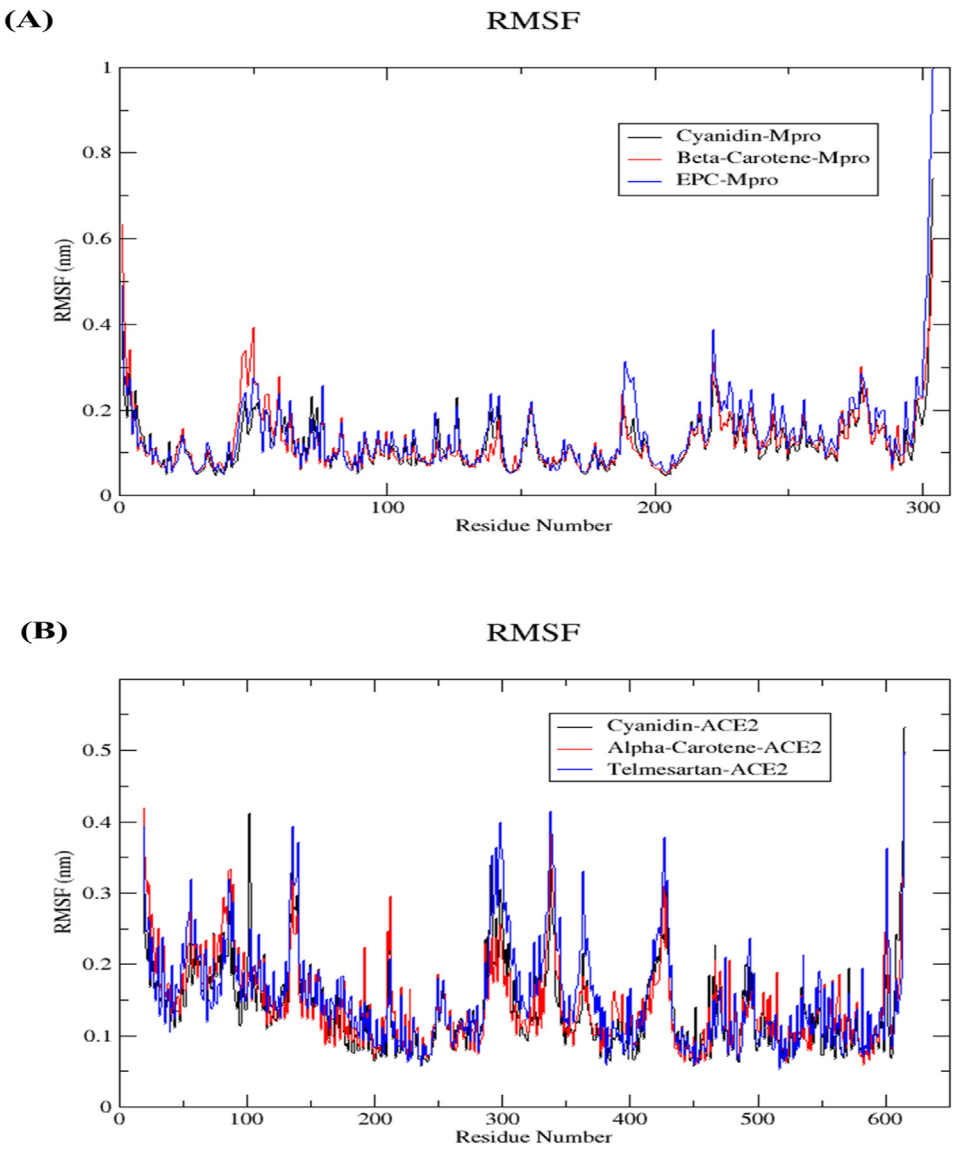

Fig. 8. (A) The RMSF of the Cyanidin-6Y84, Beta-carotene-6Y84 and EPC-6Y84 complexes during 50,000 ps simulation. **(B)** The RMSF of the Protein at-oms of cyanidin-1R42, alpha-carotene-1R42, and telmisartan-1R42 complexes during 50,000 ps simulation.

Ile152, Asp153, Ile249, and Phe294 of active pocket of SARS-CoV-2 M^{pro}. Whereas, the interaction of other top scoring carotenoids *i.e.*, α-carotene, lutein, delta-carotene, violaxanthin, neoxanthin, and γ-carotene with SARS-CoV-2 M^{pro} was favored by ΔG of −6.45, −6.14, −6.01, −5.54, −5.50, and −5.30 kcal/mol, respectively. The binding of top scoring carotenoids involved some common residues of the active pocket of SARS-CoV-2 *i.e.*, Val104, Arg105, Gln107, Pro108, Gln110, Asn151, Ile152, Asp153, Tyr154, Ile249, Phe294, Arg298, Val303, and Thr304. The strong binding of carotenoids with SARS-CoV-2 M^{pro} was also supported by low inhibition constant (*Ki*) ranging from 11.32 μM to 718.37 μM for the top 10 carotenoids and six among them exhibited *Ki* less than 100 μM (Fig. 1 and Table 3).

On the other hand, screening of polyphenols also showed potent inhibition of SARS-CoV-2 M^{pro} with ΔG values ranging from −7.24 to −4.04 kcal/mol and *Ki* of as lesser as 4.92 μM to 1.09 mM, while five polyphenols with top binding energies exhibited the *Ki* less than 10 μM, hence signifying the strong inhibition of SARS-CoV-2 M^{pro}. Among the screened polyphenols, cyanidin occupied the active pocket of SARS-CoV-2 M^{pro} with the highest ΔG of −7.24 to −4.04 kcal/mol. The binding of cyanidin was facilitated by Met006, Ala007, Phe008, Pro009, Gln127, Asp295, Arg298, Gln299, Val301, Gly302, and Thr304 residues of SARS-CoV-2 M^{pro}. The binding of polyphenols with SARS-Cov-2 M^{pro} was facilitated by several common residues *i.e.*, Met006, Ala007, Phe008, Pro009, Gln127, Asp295, Arg298, Gln299, Val301, Gly302, and Thr304 (Fig. 2). The binding pattern of carotenoids and polyphenols from *S. lycopersicum* L. with this target are similar to that of reported for other natural secondary metabolites.[63,64]

Most interestingly, the residues stabilizing the binding of top scoring carotenoid (β-carotene) against SARS-CoV-2 M^{pro} were different than that of top scoring polyphenol (cyanidin) suggesting that these potent inhibitors of SARS-CoV-2 M^{pro} can be used synergistically to produce enhanced synergistic protective effects against SARS-CoV-2 infection via restricting the proteolysis of polyproteins and thereby restricting the expression of SARS-CoV-2 viral proteins/enzymes as reported by others.[10,13] In contrast, the reference standard, EPC, did not show strong binding against SARS-CoV-2 M^{pro} active pocket (ΔG: −4.78 kcal/mol; *Ki*: 267.49 μM) and the complex was stabilized by the interaction with Lys005, Met006, Phe008, Gln127, Glu290, Phe291, Asp295, Arg298, Gln299, and Val303 residues of the same. These findings are well supported by the findings reported in previous studies.[63]

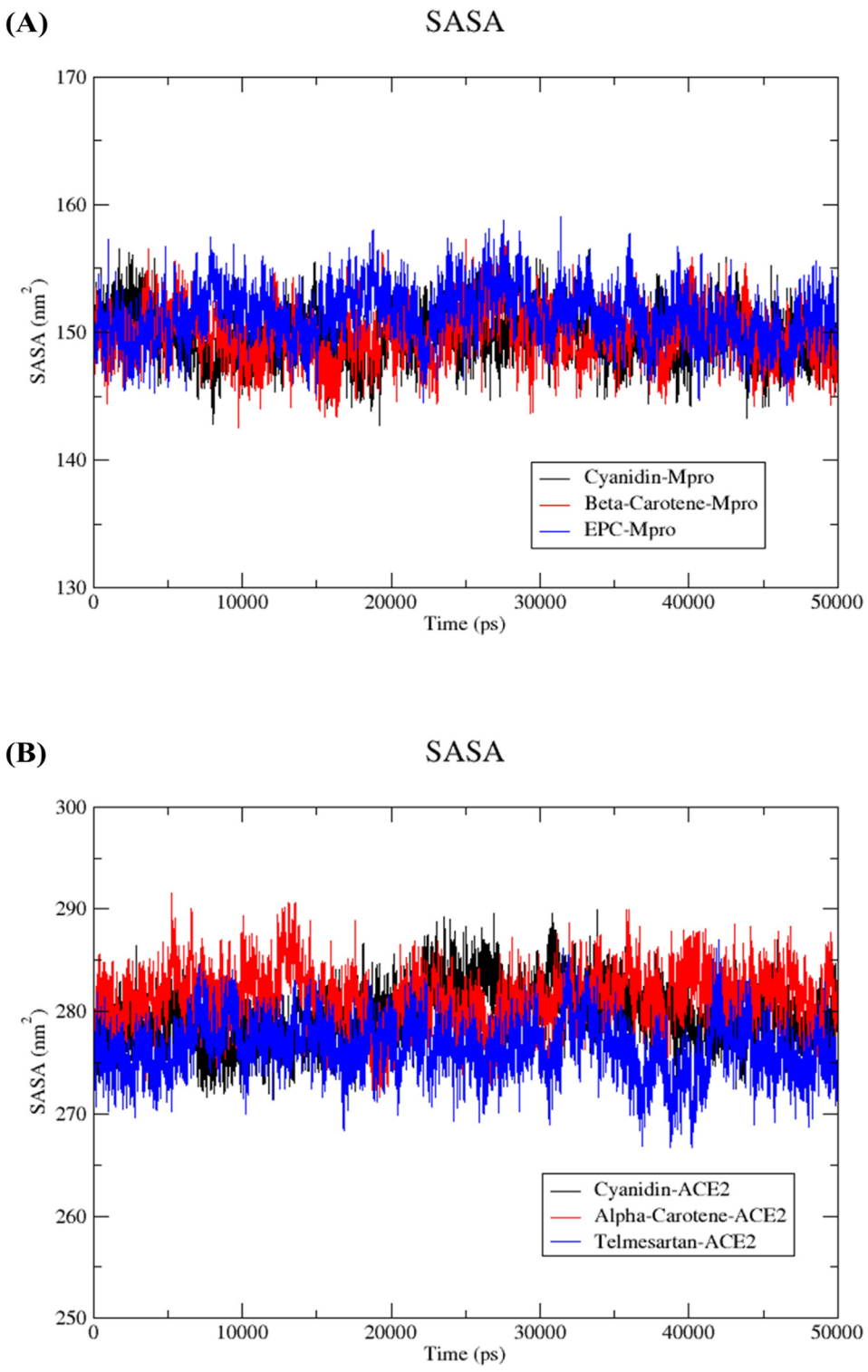

Fig. 9. (A) The SASA of the Cyanidin-6Y84, Beta-carotene-6Y84 and EPC-6Y84 complexes during 50,000 ps simulation. **(B)** The SASA area of the cyanidin-1R42, alpha-carotene-1R42, and telmisartan-1R42 complexes during 50,000 ps simulation.

Surprisingly, the binding affinity of EPC was nowhere comparable to the binding affinities of either of the top scoring carotenoids or polyphenols against SARS-CoV-2 M^{pro} (Fig. 3). The current report discovered that β-carotene, α-carotene, lutein, delta-carotene, violaxanthin, neoxanthin, and γ-carotene are the carotenoids which showed SARS-CoV-2 M^{pro} inhibitory activity better than the previously known reference standard, EPC. Moreover, eleven of the fourteen selected polyphenols (*i.e.*, cyanidin, myricetin, delphinidin, pelargonidin, quercetin, kaempferol, rutin, naringenin, chlorogenic acid, keamferol-3-rutinoside, and naringenin chalcone) also showed better inhibitory activity against SARS-CoV-2 M^{pro}, when compared to the standard inhibitor. To sum up the whole, the current study established carotenoids as well as polyphenols from *S. lycopersicum* L. as superior inhibitors of SARS-CoV-2 M^{pro} activity and fine substitutes for EPC.

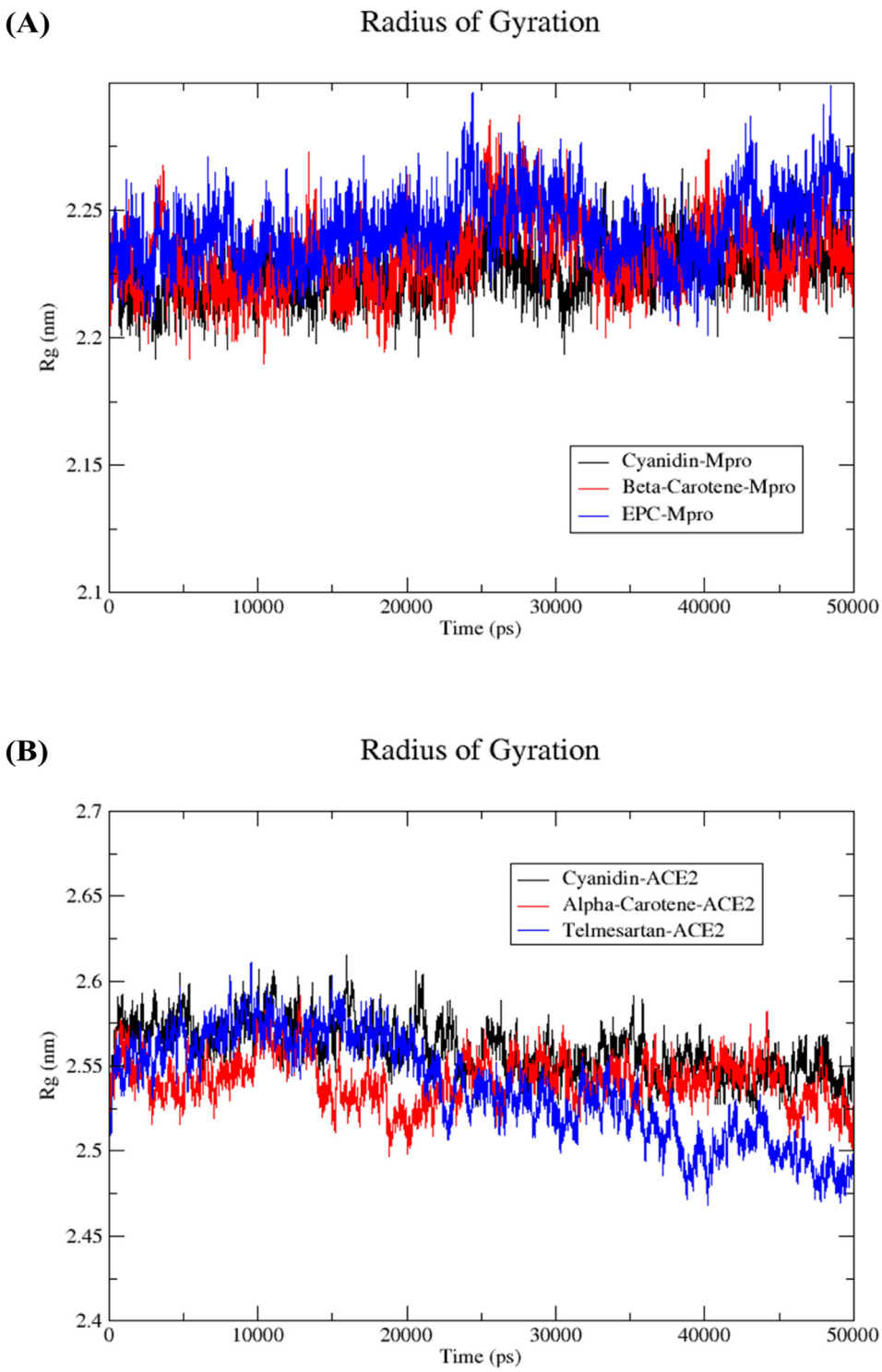

Fig. 10. (A) Radius of gyration of the of the Cyanidin-6Y84, Beta-carotene-6Y84 and EPC-6Y84 complexes during 50,000 ps simulation. **(B)** Radius of gyration of the cyanidin-1R42, alpha-carotene-1R42, and telmisartan-1R42 complexes during 50,000 ps of molecular dynamics simulation.

3.5. Human ACE-2 is inhibited by carotenoids and polyphenols from S. lycopersicum L

Extensive research on the invasion mechanism of SARS-CoV-2 has established that the RBD of the spike protein aids in the recognition of ACE-2 by SARS-CoV-2 and subsequent internalization as well as fusion with lysosomal membranes.[65,66] These observations have proven ACE-2 as one of the most preferred therapeutic targets in the management of deadly SARS-CoV-2 infection as the antagonists for this receptors (*i.e.*, telmisartan) have clinically been tested and approved for human use.[5] However, therapeutic blockage of ACE-2 with these antagonists has shown some serious adverse effects in patients already suffering from metabolic syndrome, hence signifying the importance of alternative ACE-2 antagonists. In the same context, we investigated the ACE-2 inhibitory effects of carotenoids and polyphenols from *S. lycopersicum* L. In this attempt, we found that all the selected carotenoids showed significant binding efficiency (ΔG: −8.85 to −4.49 kcal/mol; ki: 490 nM to 511.45 μM) against the active pocket of human ACE-2 crystal structure

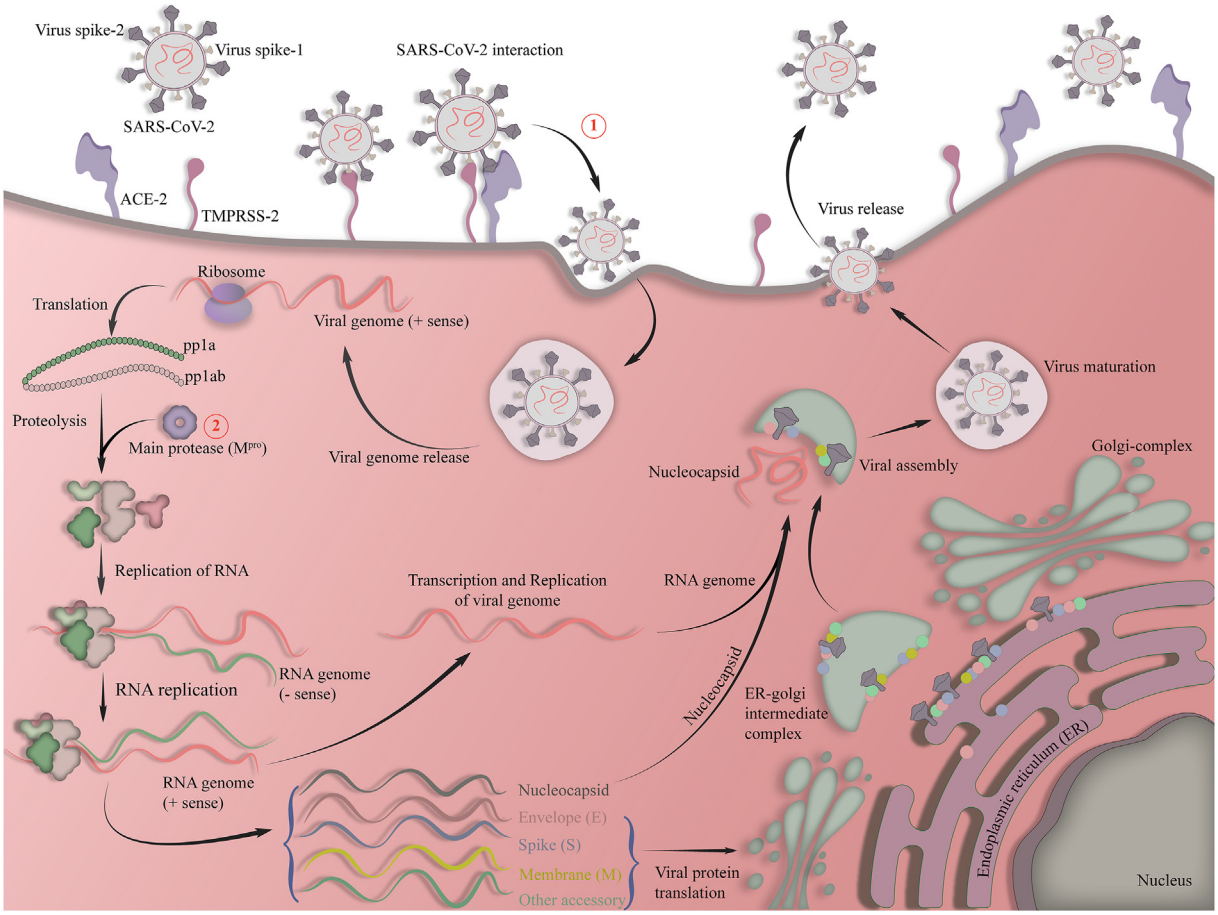

Fig. 11. Protective mechanisms of selected carotenoids and polyphenols to combat SARS-CoV-2 infection. Selected carotenoids and polyphenols blocked the entry of SARS-CoV-2 via inhibition of ACE-2 activity (1), and SARS-Cov-2 M^{pro}-mediated replication of viral replication (2).

(Table 4). Among other carotenoids, α-carotene showed the highest affinity for human ACE-2 (ΔG: −8.85 kcal/mol) and such strong interaction was supported by the involvement of Asp67, Ser70, Ala71, Leu73, Lys74, Leu95, Gln98, Ala99, Leu100, Gln102, Asp206, Leu391, and Lys562 residues of ACE-2.

Inhibition of human ACE-2 by α-carotene in this report is well supported by a recent study which also showed similar ΔG (−8.99 kcal/mol for hesperidin and −8.98 kcal/mol for chloroquine) against human ACE-2.[67] Interestingly, ten out of thirteen selected carotenoids exhibited ΔG of −5.00 to −8.85 kcal/mol which suggested a potent ACE-2 inhibitory effects of these inhibitors. However, the interaction of all the carotenoids with human ACE2 was favored by some common amino acid residues *i.e.*, Asn33, Phe40, Leu73, Gln98, Ala99, Leu100, Gln102, Gly205, Asp206, Phe390, Leu391, Arg393, Asn394, and Lys562 of human ACE-2. Such inhibition of human ACE-2 activity by selected carotenoids may result in diminished viral attachment to host, internalization and subsequent infection caused by SARS-CoV-2 (Fig. 4). The inhibitory effects of selected carotenoids against human ACE-2 activity are well in agreement with earlier publications reporting the ACE-2 modulatory ability of natural metabolites.[67,68]

On the other hand, polyphenols also occupied the active pocket of human ACE-2 with significant affinity (ΔG: −7.24 to −3.77 kcal/mol; *Ki*: 4.89 μM–366.57 μM). The maximum binding affinity was recorded for cyanidin which showed ΔG of −7.24 kcal/mol against human ACE-2 active pocket. The interaction of cyanidin against human ACE-2 was stabilized thorough its binding with Leu91, Leu95, Asp206, Tyr207, Glu208, Val209, Asn210, Gly211, Val212, Ala395, Asn397, Lys562, Ser563, Glu564, Pro565, and Trp566 residues of ACE-2. However, all the polyphenols interacted with several common amino acid residues of human ACE-2 *i.e.*, Gln102, Tyr196, Gly205, Asp206, Arg393, and Lys562 (Fig. 5). Such findings are well in justification with other reports deciphering the strong inhibition of ACE-2 by various natural products.[67]

In contrast, the ACE-2 inhibition by reference standard telmisartan (ΔG: −6.40 kcal/mol; *Ki*: 20.40 μM) was not as strong as reported in case of selected carotenoids and polyphenols from *S. lycopersicum* L. However, the binding of telmisartan was stabilized by the involvement of distinct amino acid residues *i.e.*, Gln102, Tyr196, Trp203, Glu205, Asn394, Gly395, Ala396, Asn397, Glu398, Tyr510, Ser511, Arg514, and Lys562 (Fig. 6). The most striking findings from the current study are the discovery of six carotenoids (namely α-carotene, γ-carotene, β-carotene, lutein, violaxanthin, and neoxanthin) and five polyphenols (namely cyanidin, kaempferol, naringenin, chlorogenic acid, and rutin) as the finer substitutes of reference standard telmisartan against human ACE-2 activity in combating SARS-CoV-2 infection. To sum up the whole, selected carotenoids and polyphenols from *S. lycopersicum* L. exhibited potent SARS-CoV-2 M^{pro} as well as host ACE-2 inhibitory activity better than that of respective standard antagonists and thus the dietary consumption of tomato-based products as well as their bioactive lead metabolites with potent antioxidant and anti-inflammatory effects may be promoted for the treatment and management of SARS-CoV-2 infection in a relatively safer and cheaper way.

3.6. Molecular dynamics simulation

Proteins are well reckoned to facilitate various structural and functional aspect of life including microbial pathogenesis through receptor-mediated internalization and subsequent replication/multiplication stages. Therefore, it's imperative to investigate the impact of selected

ligands (carotenoids and polyphenols) on the structural features and stability of SARS-CoV M^{pro} and ACE-2 so that inferences can be made whether these compounds block the internalization as well as replication of SARS-CoV M^{pro} inside the host. Nowadays, MDS is a remarkable tool to delineate the structural features of proteins at microscopic level.[69] To elucidate the mechanism of conformational changes including molecular interactions and stability of ligand–protein complexes, MD simulations were performed. The top scoring carotenoids and polyphenols with least ΔG values for SARS-CoV M^{pro} (*i.e.*, β-Carotene, cyanidin, and EPC) and ACE-2 (*i.e.*, α-carotene, cyanidin, and telmisartan) in docking studies were selected for the MD simulations for 50,000 ps. Comprehensive analysis of trajectories *i.e.*, RMSD, RMSF, Rg, SASA, and H-bond analysis of protein-ligand complexes along with standard drug were investigated.

3.6.1. Protein-ligand complexes were stabilized by low RMSD

The RMSD was analysed to depict the variations in backbone C_α-atoms of target proteins caused by the binding of top-ranking carotenoids and polyphenols along with their respective reference standards.[69] In ideal circumstances, the values of RMSD tend to be zero, however, it's not possible for a protein to have a RMSD of zero due to the statistical uncertainties, therefore, the RMSD <0.25 nm is considered desirable and very similar to that in case of wild proteins.[69] Lower RMSD also infers the stability of protein-ligand-complexes. In the present study, the RMSD of ligand–protein complexes were substantially reduced during the simulations and thus had high stability (Fig. 7). The RMSDs of back bone atoms of cyanidin- M^{pro}, β-carotene-M^{pro} and EPC-M^{pro} complexes were calculated to be between 0.1 and 0.4 nm. Briefly, the average RMSDs of backbone atoms for cyanidin-M^{pro} and β-carotene-M^{pro} complexes were 0.199 and 0.189 respectively, whereas the average RMSD for EPC-M^{pro}-complex was found to be 0.230. These findings clearly indicated that β-carotene-M^{pro}-complex was the most stable complex, when compared to the cyanidin-M^{pro} and EPC-M^{pro} complexes. On the other hand, the RMSDs of back bone atoms of cyanidin-ACE-2, α-carotene-ACE-2, and telmisartan-ACE-2 complexes were fluctuating between 0.1 and 0.3 nm. The average RMSDs of the backbone atoms of cyanidin-ACE2 and α-carotene-ACE2 complexes were 0.198 and 0.204, respectively, whereas the RMSDs of the backbone atoms of telmisartan-ACE2-complex was 0.183. These observations advocated that telmisartan-ACE2-complex was the most stable complex when compared to the corresponding cyanidin-ACE-2 and α-carotene-ACE-2 complexes.

3.6.2. RMSF in protein-ligand complexes

Unlike RMSD, which refers to the positional variations between entire structures as a function of time, RMSF reflects the propensity of each and every amino acid residue to fluctuate under simulation and predicts the position of the key residue/s responsible for fluctuations in a given protein70. Therefore, a comprehensive study of RMSFs of best ligand–-protein complexes were examined to determine the flexibility of amino acids within the active pocket site in protein. The variation in peaks throughout the simulation runs revealed the fluctuating regions inside the protein. The RMSF values of the corresponding amino acids in all the complexes were smaller than standard drug complexes indicating that the complexes had lower mobility, and thus ensuring the formation of a more stable enzyme–inhibitor complex (Fig. 8).

3.6.3. Solvent accessible surface area

In addition to the native forces, the globular proteins are stabilized in solutions thanks to hydrophobic interactions among non-polar residues which tend to reside there in the protein core, whereas, polar residues are exposed to the chemical milieu of the hydrophilic environment.[71] The structural aberrations to the proteins, particularly unfolding and aggregation, can be monitored via implying a set of physicochemical approaches which can monitor the hydration as well as disruption of the hydrophobic interactions at core.[23,72] This exposure of hydrophobic cores of the proteins to the antipolar environment due to the structural loss leads to the enhanced solvent accessible surface area (SASA) and can be determined through computer aided simulations.[38] On contrary, the lower the SASA value, higher the stability of protein owing to its enhanced exposure to the hydrophobic environment. Similarly, the SASA of cyanidin-6Y84, β-carotene-6Y84 and EPC-6Y84, cyanidin-1R42, α-carotene-1R42, and telmisartan-1R42, complexes were analysed during the 50,000 ps long simulations run. Results from the SASA analysis are represented in Fig. 9. The SASA scores for the cyanidin-M^{pro} and β-carotene-M^{pro} complexes were 149.73 and 149.77 nm^2, respectively, whereas the average SASA score for EPC-M^{pro}-complex was found to be 151.26 nm^2. On the other hand, the average SASA score for the cyanidin-ACE-2 and α-carotene-ACE-2 complexes were 279.61 and 281.35 nm^2, respectively, whereas the average SASA score for the telmisartan-ACE2-complex was 276.39 nm^2. These observations further validated our findings from the above-mentioned RMSD analysis that telmisartan-ACE2-complex was the most stable complex when compared to the corresponding cyanidin-ACE-2 and α-carotene-ACE-2 complexes. The findings from SASA analysis can also be correlated with the observed TPSA values as the TPSA for the cyanidin, α-carotene, and β-carotene was found to be 1.94, 13.65, and 13.54 $Å^2$, respectively, whereas TPSA for EPC and telmisartan was 48.71 and 72.94 $Å^2$, respectively.

3.6.4. Radius of gyration

The stability of SARS-CoV-2 M^{pro} and human ACE-2 complexed with the ligands with best binding energies was also investigated through the Rg as a measure of size and compactness. The magnitude of Rg negatively correlates with the stability of the proteins.[69] The calculated Rg values of all complexes decreased over the 50,000 ps long simulation runs, indicating the protein became denser after forming the complex (Fig. 10). This in turn ensures the significant comparable structural compactness and stability of all complexes. However, this is the initial study purely based on *in-silico* approach and needs to be validated through *in-vitro* and *in-vivo* studies in infection-induced models. In addition, predicted ADME, cytotoxicity and binding patterns of selected carotenoids and polyphenols through AI-based approaches might differ in experimental settings.

4. Conclusion

The worldwide spread of novel SARS-CoV-2 and associated fatalities have alarmed the discovery of effective therapeutic regimens to combat Covid-19. The current study aimed to investigate the SARS-CoV-2 M^{pro} and human ACE-2 inhibitory potential of carotenoids and polyphenols from *S. lycopersicum* L. The drug likeness studies revealed the suitability of selected compounds for drug development process as they passed the Lipinski's rules as well as ADME determinants. Further, i*n-silico* molecular modelling studies revealed that β-carotene (among other carotenoids), and cyanidin (from the polyphenols) were the best inhibitors of SARS-CoV-2 M^{pro}. Similarly, α-carotene from carotenoids and cyanidin from polyphenols exhibited strongest binding affinity against human ACE-2. In contrast, the SARS-CoV-2 M^{pro} and human ACE-2 inhibitory effects of carotenoids and polyphenols in the present report were better than that of reported in case of standard EPC, the known inhibitors of SARS-CoV-2 M^{pro} and human ACE-2, respectively. Further exploration via MDS studies also validated the dynamic behavior and stability of protein-ligand complexes as evident by desirable RMSD, RMSF, Rg, and SASA. In conclusion, the current study established carotenoids and polyphenols from *S. lycopersicum* L. as finer substitutes of reference standards against SARS-CoV-2 M^{pro} and human ACE-2 activity in combating SARS-CoV-2 infection (Fig. 11). This initial study is purely based on *in-silico* approach and needs to be validated through *in-vitro* and *in-vivo* studies in infection-induced models.

Data availability statement

All data produced in the current study are included in this published article as well as supplied as supplementary material.

CRediT authorship contribution statement

Parvej Ahmad: Conceptualization, Investigation, Methodology, Software, Visualization, Writing – original draft, Data curation, Formal analysis. **Sahir Sultan Alvi:** Conceptualization, Data curation, Formal analysis, Investigation, Project administration, Supervision, Validation, Visualization, Writing – original draft, Writing – review & editing. **Inamul Hasan:** Data curation, Formal analysis, Investigation, Methodology, Software, Writing – original draft. **M. Salman Khan:** Data curation, Formal analysis, Resources, Validation.

Declaration of competing interest

The authors declare the following financial interests/personal relationships which may be considered as potential competing interests: Sahir Sultan Alvi reports financial support was provided by Department of Health Research (DHR), MoHFW, Govt. of India. YSS Project No. 12014-13-2019-HR.

Acknowledgements

The Integral University, Lucknow is highly acknowledged for providing the necessary research facilities at IIRCs. Dr. SS Alvi is highly indebted to the DHR, MoHFW, GOI for providing the prestigious Young Scientist Fellowship/Grant (YSS Project No.: 12014/13/2019-HR). The support from the DST, India to the Department of Biosciences under the FIST program is also highly acknowledged.

Appendix A. Supplementary data

Supplementary data to this article can be found online at https://doi.org/10.1016/j.ipha.2023.10.008.

References

1. Hu B, Guo H, Zhou P, Shi ZL. Characteristics of SARS-CoV-2 and COVID-19. *Nat Rev Microbiol*. 2021;19(3):141–154. https://doi.org/10.1038/s41579-020-00459-7.
2. Chen N, Zhou M, Dong X, et al. Epidemiological and clinical characteristics of 99 cases of 2019 novel coronavirus pneumonia in Wuhan, China: a descriptive study. *Lancet*. 2020;395(10223):507–513. https://doi.org/10.1016/S0140-6736(20)30211-7.
3. Lu R, Zhao X, Li J, et al. Genomic characterisation and epidemiology of 2019 novel coronavirus: implications for virus origins and receptor binding. *Lancet*. 2020;395(10224):565–574. https://doi.org/10.1016/S0140-6736(20)30251-8.
4. Chan JFW, Kok KH, Zhu Z, et al. Genomic characterization of the 2019 novel human-pathogenic coronavirus isolated from a patient with atypical pneumonia after visiting Wuhan. *Emerg Microb Infect*. 2020;9(1):221–236. https://doi.org/10.1080/22221751.2020.1719902.
5. Hoffmann M, Kleine-Weber H, Schroeder S, et al. SARS-CoV-2 cell entry depends on ACE2 and TMPRSS2 and is blocked by a clinically proven protease inhibitor. *Cell*. 2020;181(2):271–280.e8. https://doi.org/10.1016/j.cell.2020.02.052.
6. Lan J, Ge J, Yu J, et al. Structure of the SARS-CoV-2 spike receptor-binding domain bound to the ACE2 receptor. *Nature*. 2020;581(7807):215–220. https://doi.org/10.1038/s41586-020-2180-5.
7. Bian J, Li Z. Angiotensin-converting enzyme 2 (ACE2): SARS-CoV-2 receptor and RAS modulator. *Acta Pharm Sin B*. 2021;11(1):1–12. https://doi.org/10.1016/j.apsb.2020.10.006.
8. Davidson AM, Wysocki J, Batlle D. Interaction of SARS-CoV-2 and other coronavirus with ACE (angiotensin-converting enzyme)-2 as their main receptor: therapeutic implications. *Hypertension*. 2020;76(5):1339–1349. https://doi.org/10.1161/HYPERTENSIONAHA.120.15256.
9. Tahir ul Qamar M, Alqahtani SM, Alamri MA, Chen LL. Structural basis of SARS-CoV-2 3CLpro and anti-COVID-19 drug discovery from medicinal plants. *J Pharm Anal*. 2020;10(4):313–319. https://doi.org/10.1016/j.jpha.2020.03.009.
10. Ullrich S, Nitsche C. The SARS-CoV-2 main protease as drug target. *Bioorg Med Chem Lett*. 2020;30(17):127377. https://doi.org/10.1016/j.bmcl.2020.127377.
11. Muramatsu T, Takemoto C, Kim YT, et al. SARS-CoV 3CL protease cleaves its C-terminal autoprocessing site by novel subsite cooperativity. *Proc Natl Acad Sci U S A*. 2016;113(46):12997–13002. https://doi.org/10.1073/pnas.1601327113.
12. Zhang L, Lin D, Sun X, et al. Crystal structure of SARS-CoV-2 main protease provides a basis for design of improved α-ketoamide inhibitors. *Science*. 2020;368(6489):409–412. https://doi.org/10.1126/science.abb3405.
13. Keretsu S, Bhujbal SP, Cho SJ. Rational approach toward COVID-19 main protease inhibitors via molecular docking, molecular dynamics simulation and free energy calculation. *Sci Rep*. 2020;10(1). https://doi.org/10.1038/s41598-020-74468-0.
14. Tay MZ, Poh CM, Rénia L, MacAry PA, Ng LFP. The trinity of COVID-19: immunity, inflammation and intervention. *Nat Rev Immunol*. 2020;20(6):363–374. https://doi.org/10.1038/s41577-020-0311-8.
15. Qin C, Zhou L, Hu Z, et al. Dysregulation of immune response in patients with coronavirus 2019 (COVID-19) in Wuhan, China. *Clin Infect Dis*. 2020;71(15):762–768. https://doi.org/10.1093/cid/ciaa248.
16. Xu Z, Shi L, Wang Y, et al. Pathological findings of COVID-19 associated with acute respiratory distress syndrome. *Lancet Respir Med*. 2020;8(4):420–422. https://doi.org/10.1016/S2213-2600(20)30076-X.
17. Zheng HY, Zhang M, Yang CX, et al. Elevated exhaustion levels and reduced functional diversity of T cells in peripheral blood may predict severe progression in COVID-19 patients. *Cell Mol Immunol*. 2020;17(5):541–543. https://doi.org/10.1038/s41423-020-0401-3.
18. Ahmad P, Alvi SS, Iqbal D, Khan MS. Insights into pharmacological mechanisms of polydatin in targeting risk factors-mediated atherosclerosis. *Life Sci*. 2020;254:117756. https://doi.org/10.1016/j.lfs.2020.117756.
19. Akhter F, Alvi SS, Ahmad P, Iqbal D, Alshehri BM, Khan MS. Therapeutic efficacy of Boerhaavia diffusa (Linn.) root methanolic extract in attenuating streptozotocin-induced diabetes, diabetes-linked hyperlipidemia and oxidative-stress in rats. *Biomed Res Ther*. 2019;6(7):3293–3306. https://doi.org/10.15419/bmrat.v6i7.556.
20. Ahmad P, Alvi SS, Khan MS. Functioning of organosulfur compounds from garlic (allium sativum linn) in targeting risk factor-mediated atherosclerosis: a cross talk between alternative and modern medicine. In: *Natural Bio-Active Compounds*. Springer Singapore; 2019:561–585. https://doi.org/10.1007/978-981-13-7154-7_20.
21. Alvi SS, Ahmad P, Ishrat M, Iqbal D, Khan MS. Secondary metabolites from rosemary(Rosmarinus officinalis L.): structure, biochemistry and therapeutic implications against neurodegenerative diseases. *Natural Bio-Active Compounds: Chemistry, Pharmacology and Health Care Practices*. 2019;2:1–24. https://doi.org/10.1007/978-981-13-7205-6_1. Springer Singapore.
22. Nabi R, Alvi SS, Shah A, et al. Modulatory role of HMG-CoA reductase inhibitors and ezetimibe on LDL-AGEs-induced ROS generation and RAGE-associated signalling in HEK-293 Cells. *Life Sci*. 2019;235:116823. https://doi.org/10.1016/j.lfs.2019.116823.
23. Nabi R, Alvi SS, Khan RH, Ahmad S, Ahmad S, Khan MS. Antiglycation study of HMG-R inhibitors and tocotrienol against glycated BSA and LDL: a comparative study. *Int J Biol Macromol*. 2018;116:983–992. https://doi.org/10.1016/j.ijbiomac.2018.05.115.
24. Hashim A, Alvi SS, Ansari IA, Salman Khan M. Phyllanthus virgatus forst extract and it's partially purified fraction ameliorates oxidative stress and retino-nephropathic architecture in streptozotocin-induced diabetic rats. *Pak J Pharm Sci*. 2019;32(6):2697–2708. https://doi.org/10.36721/PJPS.2019.32.6.REG.2697-2708.1.
25. Wang G, Liu Z, Li M, et al. Ginkgolide B mediated alleviation of inflammatory cascades and altered lipid metabolism in HUVECs via targeting PCSK-9 expression and functionality. *BioMed Res Int*. 2019;2019. https://doi.org/10.1155/2019/7284767.
26. Khushtar M, Siddiqui HH, Dixit RK, Alvi SS. Curative effects of triphala extract against swim stress-induced gastric ulcers via reduced ulcer index, strengthened gastric mucosa and improved redox state in rats. *Indian J Pharmaceut Sci*. 2023;85(1):176–188. https://doi.org/10.36468/pharmaceutical-sciences.1080.
27. Alvi SS, Ansari IA, Ahmad MK, Iqbal J, Khan MS. Lycopene amends LPS induced oxidative stress and hypertriglyceridemia via modulating PCSK-9 expression and Apo-CIII mediated lipoprotein lipase activity. *Biomed Pharmacother*. 2017;96:1082–1093. https://doi.org/10.1016/j.biopha.2017.11.116.
28. Alvi SS, Ansari IA, Khan I, Iqbal J, Khan MS. Potential role of lycopene in targeting proprotein convertase subtilisin/kexin type-9 to combat hypercholesterolemia. *Free Radic Biol Med*. 2017;108:394–403. https://doi.org/10.1016/j.freeradbiomed.2017.04.012.
29. Waiz M, Alvi SS, Khan MS. Potential dual inhibitors of PCSK-9 and HMG-R from natural sources in cardiovascular risk management. *EXCLI J*. 2022;21:47–76. https://doi.org/10.17179/EXCLI2021-4453.
30. Martí R, Roselló S, Cebolla-Cornejo J. Tomato as a source of carotenoids and polyphenols targeted to cancer prevention. *Cancers*. 2016;8(6). https://doi.org/10.3390/cancers8060058.
31. Alvi SS, Iqbal D, Ahmad S, Khan MS. Molecular rationale delineating the role of lycopene as a potent HMG-CoA reductase inhibitor: in vitro and in silico study. *Nat Prod Res*. 2016;30(18):2111–2114. https://doi.org/10.1080/14786419.2015.1108977.
32. Alvi SS, Ansari IA, Khan MS. Pleiotropic role of lycopene in protecting various risk factors mediated atherosclerosis. *Ann Phytomed*. 2015;4(1):54–60.
33. Ahmad P, Alvi SS, Iqbal J, Khan MS. Target-based virtual and biochemical screening against HMG-CoA reductase reveals allium sativum-derived organosulfur compound N-acetyl cysteine as a cardioprotective agent. *Rev Bras Farmacogn*. 2022:1–12. https://doi.org/10.1007/s43450-022-00330-1. Published online October 27.
34. Ahmad P, Alvi SS, Iqbal J, Khan MS. Identification and evaluation of natural organosulfur compounds as potential dual inhibitors of α-amylase and α-glucosidase activity: an in-silico and in-vitro approach. *Med Chem Res*. 2021;30(12):2184–2202. https://doi.org/10.1007/s00044-021-02799-2.
35. Asif M, Alvi SS, Azaz T, et al. Novel functionalized spiro [Indoline-3,5′-pyrroline]-2,2′dione derivatives: synthesis, characterization, drug-likeness, ADME, and anticancer potential. *Int J Mol Sci*. 2023;24(8):7336. https://doi.org/10.3390/ijms24087336.
36. Ahmad S, Nabi R, Alvi SS, et al. Carvacrol protects against carbonyl osmolyte-induced structural modifications and aggregation to serum albumin: insights from physicochemical and molecular interaction studies. *Int J Biol Macromol*. 2022;213:663–674. https://doi.org/10.1016/j.ijbiomac.2022.05.198.

37. Ahmad P, Alvi SS, Waiz M, Khan MS, Ahmad S, Khan MS. Naturally occurring organosulfur compounds effectively inhibits PCSK-9 activity and restrict PCSK-9-LDL-receptor interaction via in-silico and in-vitro approach. *Nat Prod Res*. 2023:1–10. https://doi.org/10.1080/14786419.2023.2269465. Published online.
38. Zhang D, Lazim R. Application of conventional molecular dynamics simulation in evaluating the stability of apomyoglobin in urea solution. *Sci Rep*. 2017;7(1):44651. https://doi.org/10.1038/srep44651.
39. Schneider P, Walters WP, Plowright AT, et al. Rethinking drug design in the artificial intelligence era. *Nat Rev Drug Discov*. 2020;19(5):353–364. https://doi.org/10.1038/s41573-019-0050-3.
40. Hessler G, Baringhaus KH. Artificial intelligence in drug design. *Molecules*. 2018;23(10):2520. https://doi.org/10.3390/molecules23102520.
41. Milani A, Basirnejad M, Shahbazi S, Bolhassani A. Carotenoids: biochemistry, pharmacology and treatment. *Br J Pharmacol*. 2017;174(11):1290–1324. https://doi.org/10.1111/bph.13625.
42. Pajouhesh H, Lenz GR. Medicinal chemical properties of successful central nervous system drugs. *NeuroRx*. 2005;2(4):541–553. https://doi.org/10.1602/neurorx.2.4.541.
43. Hitchcock SA, Pennington LD. Structure-brain exposure relationships. *J Med Chem*. 2006;49(26):7559–7583. https://doi.org/10.1021/jm060642i.
44. Ditzinger F, Price DJ, Ilie AR, et al. Lipophilicity and hydrophobicity considerations in bio-enabling oral formulations approaches – a PEARRL review. *J Pharm Pharmacol*. 2019;71(4):464–482. https://doi.org/10.1111/JPHP.12984.
45. Prasanna S, Doerksen R. Topological polar surface area: a useful descriptor in 2D-QSAR. *Curr Med Chem*. 2008;16(1):21–41. https://doi.org/10.2174/092986709787002817.
46. Ma XL, Chen C, Yang J. Predictive model of blood-brain barrier penetration of organic compounds. *Acta Pharmacol Sin*. 2005;26(4):500–512. https://doi.org/10.1111/j.1745-7254.2005.00068.x.
47. Leão RP, Cruz JV, da Costa GV, et al. Identification of new rofecoxib-based cyclooxygenase-2 inhibitors: a bioinformatics approach. *Pharmaceuticals*. 2020;13(9):1–26. https://doi.org/10.3390/ph13090209.
48. Bittermann K, Goss KU. Predicting apparent passive permeability of Caco-2 and MDCK cell-monolayers: a mechanistic modelHofmann A, ed. *PLoS One*. 2017;12(12):e0190319. https://doi.org/10.1371/journal.pone.0190319.
49. Volpe DA. Variability in caco-2 and MDCK cell-based intestinal permeability assays. *J Pharmaceut Sci*. 2008;97(2):712–725. https://doi.org/10.1002/jps.21010.
50. Yamashita S, Furubayashi T, Kataoka M, Sakane T, Sezaki H, Tokuda H. Optimized conditions for prediction of intestinal drug permeability using Caco-2 cells. *Eur J Pharmaceut Sci*. 2000;10(3):195–204. https://doi.org/10.1016/S0928-0987(00)00076-2.
51. Lundborg M, Wennberg CL, Narangifard A, Lindahl E, Norlén L. Predicting drug permeability through skin using molecular dynamics simulation. *J Contr Release*. 2018;283:269–279. https://doi.org/10.1016/j.jconrel.2018.05.026.
52. Chen CP, Chen CC, Huang CW, Chang YC. Evaluating molecular properties involved in transport of small molecules in stratum corneum: a quantitative structure-activity relationship for skin permeability. *Molecules*. 2018;23(4):911. https://doi.org/10.3390/molecules23040911.
53. Roberts JA, Pea F, Lipman J. The clinical relevance of plasma protein binding changes. *Clin Pharmacokinet*. 2013;52(1):1–8. https://doi.org/10.1007/s40262-012-0018-5.
54. Gurevich KG. Effect of blood protein concentrations on drug-dosing regimes: practical guidance. *Theor Biol Med Model*. 2013;10(1):20. https://doi.org/10.1186/1742-4682-10-20.
55. Zhao YH, Le J, Abraham MH, et al. Evaluation of human intestinal absorption data and subsequent derivation of a quantitative structure - activity relationship (QSAR) with the Abraham descriptors. *J Pharmaceut Sci*. 2001;90(6):749–784. https://doi.org/10.1002/jps.1031.
56. Wang B, Yang LP, Zhang XZ, Huang SQ, Bartlam M, Zhou SF. New insights into the structural characteristics and functional relevance of the human cytochrome P450 2D6 enzyme Structural features of CYP2D6 B. Wang et al. *Drug Metab Rev*. 2009;41(4):573–643. https://doi.org/10.1080/03602530903118729.
57. Zanger UM, Schwab M. Cytochrome P450 enzymes in drug metabolism: regulation of gene expression, enzyme activities, and impact of genetic variation. *Pharmacol Ther*. 2013;138(1):103–141. https://doi.org/10.1016/j.pharmthera.2012.12.007.
58. Teh LK, Bertilsson L. Pharmacogenomics of CYP2D6: molecular genetics, interethnic differences and clinical importance. *Drug Metabol Pharmacokinet*. 2012;27(1):55–67. https://doi.org/10.2133/dmpk.DMPK-11-RV-121.
59. Walko CM, McLeod H. Use of CYP2D6 genotyping in practice: tamoxifen dose adjustment. *Pharmacogenomics*. 2012;13(6):691–697. https://doi.org/10.2217/pgs.12.27.
60. Neves Cruz J, Santana De Oliveira M, Gomes Silva S, et al. Insight into the interaction mechanism of nicotine, NNK, and NNN with cytochrome P450 2A13 based on molecular dynamics simulation. *J Chem Inf Model*. 2020;60(2):766–776. https://doi.org/10.1021/acs.jcim.9b00741.
61. Sacco MD, Ma C, Lagarias P, et al. Structure and inhibition of the SARS-CoV-2 main protease reveal strategy for developing dual inhibitors against Mpro and cathepsin L. *Sci Adv*. 2020;6(50):eabe0751. https://doi.org/10.1126/SCIADV.ABE0751.
62. Zaki AA, Ashour A, Elhady SS, Darwish KM, Al-Karmalawy AA. Calendulaglycoside A showing potential activity against SARS-CoV-2 main protease: molecular docking, molecular dynamics, and SAR studies. *J Tradit Complement Med*. 2021. https://doi.org/10.1016/J.JTCME.2021.05.001. Published online May 17.
63. Bharadwaj S, El-Kafrawy SA, Alandijany TA, et al. Structure-based identification of natural products as sars-cov-2 mpro antagonist from echinacea angustifolia using computational approaches. *Viruses*. 2021;13(2). https://doi.org/10.3390/v13020305.
64. Vardhan S, Sahoo SK. Virtual screening by targeting proteolytic sites of furin and TMPRSS2 to propose potential compounds obstructing the entry of SARS-CoV-2 virus into human host cells. *J Tradit Complement Med*. 2021. https://doi.org/10.1016/j.jtcme.2021.04.001. Published online.
65. Shang J, Wan Y, Luo C, et al. Cell entry mechanisms of SARS-CoV-2. *Proc Natl Acad Sci USA*. 2020;117(21):11727–11734. https://doi.org/10.1073/PNAS.2003138117.
66. Sungnak W, Huang N, Bécavin C, et al. SARS-CoV-2 entry factors are highly expressed in nasal epithelial cells together with innate immune genes. *Nat Med*. 2020;26(5):681–687. https://doi.org/10.1038/s41591-020-0868-6, 2020 265.
67. Basu A, Sarkar A, Maulik U. Molecular docking study of potential phytochemicals and their effects on the complex of SARS-CoV2 spike protein and human ACE2. *Sci Rep*. 2020;10(1):1–15. https://doi.org/10.1038/s41598-020-74715-4.
68. Abubakar MB, Usman D, El-Saber Batiha G, et al. Natural products modulating angiotensin converting enzyme 2 (ACE2) as potential COVID-19 therapies. *Front Pharmacol*. 2021;12:629935. https://doi.org/10.3389/fphar.2021.629935.
69. Arnittali M, Rissanou AN, Harmandaris V. Structure of biomolecules through molecular dynamics simulations. *Procedia Comput Sci*. 2019;156:69–78. https://doi.org/10.1016/J.PROCS.2019.08.181.
70. Martínez L. Automatic identification of mobile and rigid substructures in molecular dynamics simulations and fractional structural fluctuation analysis. *Kleinjung J, ed. PLoS One*. 2015;10(3):e0119264. https://doi.org/10.1371/journal.pone.0119264.
71. Alvi SS, Nabi R, Khan MS, Akhter F, Ahmad S, Khan MS. Glycyrrhizic acid scavenges reactive carbonyl species and attenuates glycation-induced multiple protein modification: an in vitro and in silico study. In: Tatone C, ed. *Oxid Med Cell Longev*. 2021. 2021:1–14. https://doi.org/10.1155/2021/7086951.
72. Nabi R, Alvi SS, Shah MS, et al. A biochemical & biophysical study on in-vitro anti-glycating potential of iridin against D-Ribose modified BSA. *Arch Biochem Biophys*. 2020;686:108373. https://doi.org/10.1016/j.abb.2020.108373.